Singularity-Free Dislocation Dynamics with Strain Gradient Elasticity

Article *in* Journal of the Mechanics and Physics of Solids · August 2014

DOI: 10.1016/j.jmps.2014.03.005

CITATIONS
42

READS
616

4 authors, including:

Giacomo Po
University of California, Los Angeles
61 PUBLICATIONS **436** CITATIONS
SEE PROFILE

Markus Lazar
Technische Universität Darmstadt
112 PUBLICATIONS **1,785** CITATIONS
SEE PROFILE

N.M. Ghoniem
University of California, Los Angeles
407 PUBLICATIONS **5,620** CITATIONS
SEE PROFILE

Journal of the Mechanics and Physics of Solids 68 (2014) 161–178

Contents lists available at ScienceDirect

Journal of the Mechanics and Physics of Solids

journal homepage: www.elsevier.com/locate/jmps

Singularity-free dislocation dynamics with strain gradient elasticity

Giacomo Po [a,*], Markus Lazar [b], Dariush Seif [a,c], Nasr Ghoniem [a]

[a] Department of Mechanical and Aerospace Engineering, University of California Los Angeles, Los Angeles, CA 90095, United States
[b] Department of Physics, Darmstadt University of Technology, Hochschulstr. 6, D-64289 Darmstadt, Germany
[c] Fraunhofer Institut für Werkstoffmechanik, Freiburg 79108, Germany

ARTICLE INFO

Article history:
Received 10 December 2013
Received in revised form
17 February 2014
Accepted 9 March 2014
Available online 22 March 2014

Keywords:
Dislocation dynamics
Gradient elasticity
Singularity
Solid angle

ABSTRACT

The singular nature of the elastic fields produced by dislocations presents conceptual challenges and computational difficulties in the implementation of discrete dislocation-based models of plasticity. In the context of classical elasticity, attempts to regularize the elastic fields of discrete dislocations encounter intrinsic difficulties. On the other hand, in gradient elasticity, the issue of singularity can be removed at the outset and smooth elastic fields of dislocations are available. In this work we consider theoretical and numerical aspects of the non-singular theory of discrete dislocation loops in gradient elasticity of Helmholtz type, with interest in its applications to three dimensional dislocation dynamics (DD) simulations. The gradient solution is developed and compared to its singular and non-singular counterparts in classical elasticity using the unified framework of eigenstrain theory. The fundamental equations of curved dislocation theory are given as non-singular line integrals suitable for numerical implementation using fast one-dimensional quadrature. These include expressions for the interaction energy between two dislocation loops and the line integral form of the generalized solid angle associated with dislocations having a spread core. The single characteristic length scale of Helmholtz elasticity is determined from independent molecular statics (MS) calculations. The gradient solution is implemented numerically within our variational formulation of DD, with several examples illustrating the viability of the non-singular solution. The displacement field around a dislocation loop is shown to be smooth, and the loop self-energy non-divergent, as expected from atomic configurations of crystalline materials. The loop nucleation energy barrier and its dependence on the applied shear stress are computed and shown to be in good agreement with atomistic calculations. DD simulations of Lomer–Cottrell junctions in Al show that the strength of the junction and its configuration are easily obtained, without ad-hoc regularization of the singular fields. Numerical convergence studies related to the implementation of the non-singular theory in DD are presented.
Published by Elsevier Ltd.

1. Introduction

Most mechanical properties of crystalline materials are controlled by the behavior and evolution of complex dislocation ensembles. This observation stands behind a long-standing goal to develop plasticity theory on a physical, rather than

* Corresponding author.
E-mail addresses: gpo@ucla.edu (G. Po), lazar@fkp.tu-darmstadt.de (M. Lazar), dariush.seif@iwm-extern.fraunhofer.de (D. Seif), ghoniem@ucla.edu (N. Ghoniem).

http://dx.doi.org/10.1016/j.jmps.2014.03.005
0022-5096/Published by Elsevier Ltd.

empirical, basis. However, the difficulty associated with averaging individual dislocation properties across many length and time scales, from atomistic to continuum, arguably makes dislocation mechanics "the most difficult remaining problem of classical physics" (Cottrell, 2002). One has therefore to resort to models limited to a specific length and time scale of observation. In this multi-scale approach, the meso-scale range (1–100 μm) is occupied by the elastic theory of discrete dislocations (Friedel, 1967; Nabarro, 1987; Hirth and Lothe, 1992). The theory has proven not only extremely effective in explaining the elastic properties of crystal dislocations, but also well suited for numerical implementation. The computational side of the theory focused on the quasi-static evolution of a given dislocation configuration is known as the Discrete Dislocation Dynamics (DD) method (Lepinoux and Kubin, 1987; Ghoniem and Amodeo, 1988; Gulluoglu et al., 1989; Kubin et al., 1992; Schwarz, 1997; Zbib et al., 1998; Ghoniem et al., 2000; Weygand, 2002; Bulatov et al., 2004). The objective of the DD method is the prediction of the mechanical response of a mesoscopic material volume containing a large number of dislocations, in response to intrinsic (dislocation configuration, material properties, grain size, etc.) and extrinsic (applied load, strain rate, temperature, etc.) factors, without resorting to ad-hoc assumptions.

Despite its successes, the classical theory of dislocations and the computational methods that descend from it face intrinsic limitations on their numerical accuracy, as well as on their ability to access resolution at the atomic length scale. Such difficulties stem from the representation of crystal dislocations by means of Volterra dislocations, a special type of elastic distortion of multiply connected solids introduced well before crystal dislocations were discovered (Volterra, 1907). A well known collateral effect of this idealization is the emergence of singularities in the elastic fields of Volterra dislocations, which limit the validity of the solution to a somewhat arbitrary region outside the dislocation core. Consequently, several fundamental physical quantities become ill-determined (e.g. self energy/stress of dislocation loops and interaction energy/stress of intersecting dislocations). In order to overcome the difficulties associated with the unphysical singular character of Volterra dislocations, various methods of regularization of the elastic solution have been proposed. In the context of standard elasticity, a first class of methods comprises efforts based on the use of cut-off radii (Brown, 1964; Gavazza and Barnett, 1976), which avoid dealing with the singularity but introduce parameters of arguable physical interpretation. In contrast, a second category of methods removes the singularity adopting the concept of distributed dislocation core (de Wit, 1960). This concept, originally introduced by the celebrated Peierls (1940)–Nabarro (1947) model of lattice resistance, can be recognized in the standard core of Lothe (1992) and the isotropic core of Cai et al. (2006). Only the latter, however, is applicable to the study of curved dislocation loops in three dimensions.

An alternative approach to overcome the issue of singularity is to consider discrete dislocations in the broader field of generalized elasticity. This is a natural choice in light of the relationship between higher order stress measures (absent in classical elasticity) and the long-range effects of interatomic forces, which has been suggested by several authors (Kröner, 1963; Toupin and Gazis, 1965; Mindlin, 1972). Generalized elastic theories of discrete dislocations have been developed in three different frameworks: micropolar (Cosserat) elasticity, non-local elasticity, and gradient elasticity. In micropolar elasticity, Kessel (1970) found solutions for screw and edge dislocations and Minagawa (1979) for dislocation loops. However, these solutions not only present the classical singularities but also add new singularities related to the presence of modified Bessel functions. Similar results are also found in Nowacki (1986) and references therein. Straight screw and edge dislocations in non-local elasticity with exponential non-local kernel were considered by Eringen (1977b) and Eringen (1977a), respectively. The solution yields regularized stress but the strain and displacement fields remain classical (singular). Similar results using a non-local kernel of Helmholtz type were found by Eringen (1983) for screw dislocations and by Eringen (1984) for dislocation loops (see also Eringen, 2002). However the Green's function of the Helmholtz bi-Laplace equation used by Eringen lacks a term which prevents the regularization of the Peach–Koehler stress (see Lazar, 2014, for details). The first effort towards a non-singular dislocation theory in the framework of gradient elasticity was carried out by Lardner (1971), who considered straight screw and edge dislocations in the framework of Mindlin's gradient elasticity (Mindlin, 1964). Considering neither plastic distortion nor dislocation density, Lardner constructed solutions to a compatible elastic boundary value problem, and consequently failed to remove the classical singularities. More than two decades later, Gutkin and Aifantis (1996, 1997) studied straight screw and edge dislocations in a model characterized by the presence of gradient terms in Hooke's law. The model predicts non-singular strains and gives rise to a smooth displacement field in proximity of the dislocation core. However, the framework of Gutkin and Aifantis (1996, 1997) lacks double stresses and, consequently, the Cauchy stress remains singular. In a refined version of the theory, Gutkin and Aifantis (1999) were able to also regularize the stress field using a more sophisticated Hooke's law. Subsequent work has further developed the non-singular theory of straight dislocations in a special version of gradient elasticity containing only one characteristic parameter, which we shall refer to as gradient elasticity of Helmholtz type (Lazar and Maugin, 2005; Lazar et al., 2005; Lazar and Maugin, 2006). Only recently has the theory been extended to curved dislocation loops in three dimensions (Lazar, 2012, 2013). These recent developments in the gradient theory of elasticity endow DD with a level of maturity that is necessary for computer simulations of 3-D dislocation ensembles with near atomic resolution.

In this work we explore the use of the non-singular gradient theory of discrete dislocations (Lazar, 2012, 2013) in three-dimensional DD simulations, and show that it provides a simple and valuable alternative to the classical theory as the foundation for numerical implementation. The first objective of the paper is to highlight differences and advantages of the gradient formulation compared to its singular and non-singular counterparts in standard elasticity. Section 2 is dedicated to this topic. As part of the discussion, we derive a closed-form expression for the interaction energy between two dislocation loops in gradient elasticity of Helmholtz type. This expression will be used to determine the non-singular self-energy of a dislocation loop. We also address the theoretical issue of converting the generalized solid angle associated with the displacement field of dislocations having distributed

core into a line integral form. A generalized Eshelby (1982)–de Wit (1981) line integral equation is developed and the conditions of its suitability for numerical implementation are discussed. Once the fundamentals have been established, in Section 3 we proceed to the second task of the paper, which is the identification of the only extra characteristic parameter required by the gradient theory. This task is achieved through the matching of the Cauchy stress produced by straight dislocations to results of molecular statics (MS) calculations. In Section 4 we consider several applications of the non-singular theory of curved dislocation loops. In particular, we compute the strength of junctions in fcc metals, and analyze the implications of the theory when applied to the prediction of homogeneous dislocation nucleation. Finally, discussion and conclusions are given in Section 5.

2. Discrete dislocation loops in elasticity

Three[1] theories of curved discrete dislocation loops in three dimensions are suitable candidates for numerical implementation. These are the classical elastic theory and the theory of Cai et al. (2006), and the gradient theory of Lazar (2012, 2013). In this section we highlight analogies and differences between the three theories using the unified viewpoint of linearized incompatible elasticity. The main kinematic assumption of the framework is that the displacement gradient $u_{i,j}$ is split additively into an elastic distortion β^E_{ij} and a plastic distortion β^P_{ij}:

$$u_{i,j} = \beta^E_{ij} + \beta^P_{ij} \tag{1}$$

In this kinematic framework, dislocations are sources of plastic distortion, and a particular form of the tensor $\boldsymbol{\beta}^P$ will be specified for each theory. Given a specific form of $\boldsymbol{\beta}^P$, we recall that the corresponding dislocation density tensor $\boldsymbol{\alpha}$ is obtained as the negative curl of $\boldsymbol{\beta}^P$: $\alpha_{ij} = -\epsilon_{jkm}\beta^P_{im,k}$.

2.1. Discrete dislocation loops in classical elasticity

The standard linear elastic medium can be characterized by a strain energy density, W, expressed as a quadratic form of the elastic distortions:

$$W = \tfrac{1}{2} c_{ijkl}\beta^E_{ij}\beta^E_{kl} \tag{2}$$

where c_{ijkl} is the standard rank-4 tensor of elastic moduli. Given W and the aforementioned assumption of linearized kinematics, the principle of virtual work demands that the displacement field, u_k, satisfies the following equilibrium equation:

$$\left(\frac{\partial W}{\partial \varepsilon^E_{ij}}\right)_{,j} = \sigma_{ij,j} = c_{ijkl}(u_{k,l} - \beta^P_{kl})_{,j} = L_{ik}u_k - c_{ijkl}\beta^P_{kl,j} = 0 \tag{3}$$

where $\sigma_{ij} = \partial W/\partial \varepsilon^E_{ij}$ is the Cauchy stress tensor, and $L_{ik} = c_{ijkl}\partial_l\partial_j$ is the Navier differential operator. Eq. (3) can be solved using the Green's function method. For an infinite medium, the displacement and stress fields read (Mura, 1987)

$$u_i = -c_{mnpq}G^0_{im,n} \ast \beta^P_{pq} \tag{4a}$$

$$\sigma_{ij} = c_{ijkl}\epsilon_{lqs}c_{mnpq}G^0_{km,n} \ast \alpha_{ps} \tag{4b}$$

In Eq. (4), G^0_{km} is the Green's function of the Navier operator and the symbol $\ast$ indicates convolution over three-dimensional space. In order to obtain a Volterra dislocation extending over a surface $\mathcal{S}$, the plastic eigendistortion is taken in following form:

$$\beta^{P0}_{kl}(\boldsymbol{x}) = -\int_{\mathcal{S}} \delta(R(\boldsymbol{x}-\boldsymbol{x}'))b_k \, dA'_l \tag{5}$$

where δ is the Dirac delta function, $R(\boldsymbol{x}) = \sqrt{\boldsymbol{x}\cdot\boldsymbol{x}}$ the Euclidean distance function, and b_i is the displacement jump across $\mathcal{S}$ (Burgers vector). Because $\boldsymbol{b}$ is constant, the dislocation density tensor turns out to be concentrated on the dislocation line, that is the closed line $\mathcal{L} = \partial\mathcal{S}$ bounding the surface $\mathcal{S}$:

$$\alpha^0_{ij}(\boldsymbol{x}) = -\epsilon_{jkm}\beta^{P0}_{im,k} = \oint_{\mathcal{L}} \delta(R(\boldsymbol{x}-\boldsymbol{x}'))b_i \, dL'_j \tag{6}$$

Letting $\boldsymbol{\beta} = \boldsymbol{\beta}^0$ in (4a) and $\boldsymbol{\alpha} = \boldsymbol{\alpha}^0$ in (4b), the displacement and stress fields of a Volterra dislocation are obtained. Limiting the attention to isotropic solids, for which G^0_{ij} depends on $\boldsymbol{x}$ only through the derivatives of $R(\boldsymbol{x})$, yields the solution:

$$u^0_i = \frac{1}{8\pi}\partial_j\Delta R \ast \beta^{P0}_{ij} - U_{ikl}R \ast \alpha^0_{kl} \quad \text{(Burgers equation)} \tag{7a}$$

$$\sigma^0_{ij} = S_{ijkl}R \ast \alpha^0_{kl} \quad \text{(Peach–Koehler stress equation)} \tag{7b}$$

[1] The (corrected) non-local theory of Eringen (1984) is also a possible candidate if one is only interested in the non-singular stress field of dislocations. However, the stress field of dislocation loops in non-local elasticity of Helmholtz type is identical to the field obtained in gradient elasticity of Helmholtz type. Therefore we do not discuss Eringen's non-local theory in this paper.

where U_{ikl} and S_{ijkl} are linear differential operators respectively defined as

$$U_{ikl}=\frac{1}{8\pi}\epsilon_{klm}\left(\delta_{im}\Delta-\frac{1}{1-\nu}\partial_i\partial_m\right)\quad S_{ijkl}=\frac{\mu}{8\pi}\left[\left(\delta_{il}\epsilon_{jmk}+\delta_{jl}\epsilon_{imk}\right)\partial_m\Delta+\frac{2}{1-\nu}\epsilon_{klm}\left(\partial_i\partial_j\partial_m-\delta_{ij}\partial_m\Delta\right)\right] \tag{8}$$

In Eq. (8), Δ is the Laplace operator, ν is the Poisson ratio, and μ is the shear modulus. Finally, it should be noticed that, in virtue of the sifting property of the Dirac-δ appearing in both β^{P0}_{ij} and α^{0}_{ij}, the calculation of the displacement field reduces to a combination of surface and line integrals, while the stress field transforms into a line integral.

Another important quantity is the elastic energy of interaction between two loops. Neglecting surface integrals that vanish at infinity, the interaction energy between two loops is

$$\begin{aligned}E_I&=\int_{\mathbb{R}^3}\sigma^{(1)}_{ij}\beta^{E0(2)}_{ij}\,dV=\int_{\mathbb{R}^3}\sigma^{(1)}_{ij}(u^{(2)}_{i,j}-\beta^{P0(2)}_{ij})\,dV=-\int_{\mathbb{R}^3}[(\sigma^{(1)}_{ij})_{,j}u^{(2)}_i+\sigma^{(1)}_{ij}\beta^{P0(2)}_{ij}]\,dV\\&=-\int_{\mathbb{R}^3}\sigma^{(1)}_{ij}\beta^{P0(2)}_{ij}\,dV=-\int_{\mathcal{S}^{(2)}}\sigma^{(1)}_{ij}b^{(2)}_i\,dA^{(2)}_j=-\int_{\mathcal{S}^{(2)}}\oint_{\mathcal{L}^{(1)}}S_{ijkl}R\;b^{(1)}_k\,dL^{(1)}_l b^{(2)}_i\,dA^{(2)}_j\end{aligned} \tag{9}$$

In the last equality, we used the Peach–Koehler stress (7b). This form can be further reduced using Stokes' theorem. Doing so, it is possible to verify that the interaction energy between two loops can be expressed in terms of the following double line integral (de Wit, 1960):

$$E_I=-\oint_{\mathcal{L}^{(2)}}\oint_{\mathcal{L}^{(1)}}M_{ijkl}R\;b^{(1)}_k\,dL^{(1)}_l b^{(2)}_i\,dL^{(2)}_j \tag{10}$$

where the differential operator M_{ijkl} is

$$M_{ijkl}=\frac{\mu}{4\pi(1-\nu)}\left[\left(\frac{1-\nu}{2}\delta_{ij}\delta_{kl}+\nu\delta_{il}\delta_{jk}-\delta_{jl}\delta_{ik}\right)\Delta+\delta_{jl}\partial_i\partial_k\right] \tag{11}$$

In this compact summary, we also wish to recall that the force df_k acting on an infinitesimal length of dislocation can be computed integrating the divergence of the Eshelby stress tensor. This construction will turn out to be useful later on for dislocations with a spread core, for which the definition of the force is not self-evident. For the classical theory, this clearly yields the standard Peach and Koehler (1950) force, in fact:

$$\int_{\mathbb{R}^3}(W\delta_{kj}-\sigma_{ij}\beta^{E}_{ik})_{,j}\,dV=\int_{\mathbb{R}^3}\epsilon_{kjm}\sigma_{ji}\alpha^{0}_{im}\,dV=\oint_{\mathcal{L}}\underbrace{\epsilon_{kjm}\sigma_{ji}b_i\,dL_m}_{df_k} \tag{12}$$

Clearly, in order to obtain the Peach–Koehler force between two dislocation loops it is sufficient to substitute the Peach–Koehler stress equation (7b) into (12).

The Burgers equation (7a), Peach–Koehler stress equation (7b), the Peach–Koehler force equation (12), and the interaction energy equation (10) are the fundamental equations that govern the quasi-static elastic theory of discrete dislocation loops (Volterra dislocations). They have been used extensively in investigating the elastic properties of crystal dislocations in metals and alloys. Nevertheless, Volterra's dislocations possess two peculiar characteristics that distinguish them from crystal dislocations. First, the displacement field is multivalued on the surface $\mathcal{S}$. Second, all fields become singular approaching the dislocation line $\mathcal{L}$. The reason behind the break down of Volterra's solution is suggested by Weingarten formulae. In fact, in order to have a discontinuous displacement field (with continuous elastic strain) over a simply connected body Ω, one must first consider the corresponding multi-valued field obtained removing a torus $\mathcal{T}$ around the dislocation line, hence making each Burgers circuit irreducible. Only then the displacement field can be made single-valued by introducing the branch cut $\mathcal{S}$ which restores simple-connectiviness of the domain $\Omega\backslash\mathcal{T}\backslash\mathcal{S}$ (see Teodosiu, 1982, ch. 2.8). This process, however, removes the region of interest (the dislocation core) from the continuum description and precludes any further possibility of referring to the elastic fields inside the dislocation core. This limitation, which is intrinsic in the definition of a Volterra dislocation, does not apply to dislocations in real crystals, which cannot yield infinite stress nor concentrated displacement jumps. These intrinsic differences between Volterra and crystal dislocations have motivated the need to develop regularization methods already discussed in the introduction.

2.2. Elastic field regularization by Cai et al.

Cai et al. (2006) developed a theory that yields non-singular interaction energy and stress between dislocation loops in closed form. Here we shall cast the original formulation of Cai et al. (2006) into the eigenstrain framework to highlight analogies and differences with respect to the classical and gradient theories. To this end, instead of a Volterra eigendistortion, we consider the following dislocation eigendistortion and the corresponding dislocation density tensor:

$$\tilde{\beta}^{P}_{ij}=\beta^{P0}_{ij}*\tilde{w}\quad\tilde{\alpha}_{ij}=-\epsilon_{jkm}\tilde{\beta}^{P}_{im,k}=\alpha^{0}_{ij}*\tilde{w} \tag{13}$$

These expressions are obtained from the corresponding classical quantities by convolution with an isotropic spreading function $\tilde{w}(R)$. With this choice, the general solution (7) yields the following displacement and stress fields of a dislocation

in an isotropic medium:

$$\tilde{u}_i = \frac{1}{8\pi}\partial_j \Delta R * \tilde{w} * \beta^{P0}_{ij} - U_{ikl} R * \tilde{w} * \alpha^0_{kl} = \frac{1}{8\pi}\partial_j \Delta \tilde{R} * \beta^{P0}_{ij} - U_{ikl}\tilde{R} * \alpha^0_{kl} \quad \text{(Burgers equation)} \tag{14a}$$

$$\tilde{\sigma}_{ij} = S_{ijpq} R * \tilde{w} * \alpha^0_{pq} = S_{ijpq}\tilde{R} * \alpha^0_{pq} \quad \text{(Peach–Koehler stress equation)} \tag{14b}$$

In Eqs. (14a) and (14b) the commutative and associative properties of the convolution have been used to introduce the modified distance function $\tilde{R} = R * \tilde{w}$. In order to understand the choice of the spreading function $\tilde{w}$, let us consider the expression of the Peach–Koehler force consistent with the theory of Cai et al. (2006). Analogous to Eq. (12), the force density is obtained from the divergence of the Eshelby stress tensor. It reads

$$\int_{\mathbb{R}^3} (W\delta_{kj} - \sigma_{ij}\beta^E_{ik})_{,j}\, dV = \int_{\mathbb{R}^3} \epsilon_{kjm}\sigma_{ji} \tilde{w} * \alpha^0_{im}\, dV = \int_{\mathbb{R}^3} \epsilon_{kjm}\sigma'_{ji}\alpha^0_{im}\, dV = \oint_{\mathcal{L}} \underbrace{\epsilon_{kjm}\sigma'_{ji} b_i\, dL_m}_{df_k} \tag{15}$$

Therefore it is seen that the force exerted per unit line of dislocation does not involve the Cauchy stress but the "effective" stress

$$\sigma'_{ij} = \sigma_{ij} * \tilde{w} \tag{16}$$

obtained by convolution of the Cauchy stress with the spreading function $\tilde{w}$. As a consequence, unlike the classical theory, the stress measure that appears in the Peach–Koehler force between two dislocation loops is not the Peach–Koehler stress but the particular expression of the effective stress, called $\boldsymbol{\sigma}^{\mathrm{ns}}$, obtained using (14b) in (16). By virtue of the distributive property of the convolution operator, this reads

$$\sigma^{\mathrm{ns}}_{ij} = \tilde{\sigma}_{ij} * \tilde{w} = S_{ijpq}\tilde{R} * \tilde{w} * \alpha^0_{pq} = S_{ijpq} R * \tilde{w} * \tilde{w} * \alpha^0_{pq} = S_{ijpq} R_a * \alpha^0_{pq} \tag{17}$$

In (17), a new spreading function w is introduced from the convolution of $\tilde{w}$ with itself ($w = \tilde{w} * \tilde{w}$) and a second modified distance function R_a is defined as $R_a = \tilde{R} * \tilde{w} = R * w$. Although the approach is general, Cai et al. (2006) suggested that the spreading function w be chosen to yield the result $R_a = \sqrt{R^2 + a^2}$, where a is the parameter that defines the size of the dislocation core. With this choice, the stress measure $\sigma^{\mathrm{ns}}_{ij}$ becomes non-singular. Similarly, the interaction energy between two loops turns out to be non-singular. In fact, following the derivation of the previous section, the energy can be expressed as

$$E^{\mathrm{ns}}_l = -\int_{\mathbb{R}^3} \tilde{\sigma}^{(1)}_{ij}\tilde{\beta}^{P(2)}_{ij}\, dV = -\oint_{\mathcal{L}^{(2)}}\oint_{\mathcal{L}^{(1)}} M_{ijkl} R_a\, b^{(1)}_k\, dL^{(1)}_l b^{(2)}_i\, dL^{(2)}_j \tag{18}$$

The procedure of Cai et al. (2006) guarantees two main advantages. The first is that both interaction stress and energy between dislocations are non-singular. The second is that R_a is simple enough that the line integrals (17) and (18) can be computed analytically for straight dislocation segments. Nonetheless, the strength of the procedure, which derives from a simple choice of w, defines also its limitations because it leaves the analytical form of $\tilde{w}$ unknown. Therefore, the fundamental equations of dislocation theory, which involve $\tilde{w}$ (Burgers equation (14a), Peach–Koehler stress (14b), Peach–Koehler force (15)) cannot be found in closed form due to the indeterminacy of $\tilde{w}$. This has several practical consequences. First, consider the Peach–Koehler force exerted on a dislocation by an "external" source of stress $\boldsymbol{\sigma}^{ext}$ (e.g. a source other than another dislocation). Then, according to (15), the force will involve an effective stress, which must be computed explicitly from its definition, (16), as $\boldsymbol{\sigma}' = \boldsymbol{\sigma}^{ext} * \tilde{w}$. This requires a computationally expensive convolution integral to be performed for each point where the Peach–Koehler force is required. Second, we point out that the non-singular stress (17) is not the correct measure of the (Cauchy) stress field generated by a dislocation at a generic field point, a misinterpretation sometimes found in the literature (e.g. Aifantis, 2009; Schoeck, 2010). The correct (Cauchy) stress is (14b), and it depends on the unknown spreading function $\tilde{w}$, which can only be computed approximately using the numerical fit of $\tilde{w}$ indicated by Cai et al. (2006). Third, although the Burgers equation yielding the displacement field of a dislocation with spread core was not given in the original work, here we show that the expression consistent with the theory is Eq. (14a). The first term in Eq. (14a) is a generalized solid angle and requires a surface integration of the vector quantity $\partial_i \Delta\tilde{R}$ over the slip area. Because in DD slip surfaces are generally not tracked, for practical applications it is necessary to convert the generalized solid angle into a line integral. In Appendix B we derive the line integral representation of the generalized solid angle for dislocations with arbitrary spread core. It is shown that the result involves symbolic manipulation of the quantity $\partial_i \Delta\tilde{R}$, which unfortunately remains unknown in the approach of Cai et al. (2006). Nevertheless, we mention that an approximate expression could be obtained using the numerical fit $\tilde{R} \approx (1-m)R_{a_1} + mR_{a_2}$, where m, a_1 and a_2 are the same constants suggested by Cai et al. (2006) to fit $\tilde{w}$. With this approximation, the line integral representation of the generalized solid angle developed in Appendix B can be used to compute the non-singular displacement field consistent with the approximation of $\tilde{R}$.

2.3. Discrete dislocation loops in gradient elasticity of Helmholtz type

The theory of gradient elasticity of Helmholtz type is governed by a strain energy density that depends on (incompatible) elastic strains and their gradients in the following form:

$$W\left(\varepsilon^E_{ij},\varepsilon^E_{ij,m}\right)=\frac{1}{2}c_{ijkl}\varepsilon^E_{ij}\varepsilon^E_{kl}+\frac{\ell^2}{2}c_{ijkl}\varepsilon^E_{ij,m}\varepsilon^E_{kl,m} \tag{19}$$

where ℓ is a characteristic internal length parameter of the material. We remark that (19) can be considered a simplified version of Mindlin and Eshel (1968) type-II form of energy density with only one characteristic length scale, and that only Mindlin type-II (strain gradient) form can be generalized from compatible to incompatible elasticity.

Given this form of W, the principle of virtual work dictates that static equilibrium be expressed in the form:

$$\left(\frac{\partial W}{\partial \varepsilon^E_{ij}}-\left(\frac{\partial W}{\partial \varepsilon^E_{ij,m}}\right)_{,m}\right)_{,j}=(\sigma_{ij}-\tau_{ijm,m})_{,j}=c_{ijkl}\partial_j\left(1-\ell^2\partial_m\partial_m\right)\left(u_{k,l}-\beta^P_{kl}\right)=L_{ik}Lu_k-Lc_{ijkl}\beta^P_{kl,j}=0 \tag{20}$$

where $\tau_{ijm}=\partial W/\partial\varepsilon^E_{ij,m}=\ell^2c_{ijkl}\varepsilon^E_{kl,m}=\ell^2\sigma_{ij,m}$ is the double stress tensor, and $L=1-\ell^2\partial_m\partial_m$ is the Helmholtz differential operator. Eq. (20) is formally similar to (3), with the difference that the composed Navier–Helmholtz operator $L_{ik}L$ replaces the Navier operator, and $L\beta^P_{kl}$ replaces β^P_{kl}. Letting G_{im} be the Green's tensor of the composed Navier–Helmholtz operator, this similarity allows us to easily find the solution of (20) as

$$u_i=-c_{mnpq}G_{im,n}*L\beta^P_{pq}=-c_{mnpq}G^0_{im,n}*G*\beta^{P0}_{pq} \tag{21a}$$

$$\sigma_{ij}=c_{ijkl}\epsilon_{lqs}c_{mnpq}G_{km,n}*L\alpha_{ps}=c_{ijkl}\epsilon_{lqs}c_{mnpq}G^0_{km,n}*G*\alpha^0_{ps} \tag{21b}$$

Notice that the last equality in both (21a) and (21b) makes use of the property that the Green's tensor G_{ij} of the composed Navier–Helmholtz operator $L_{ik}L$ is the convolution of the Green's tensors of the individual operators, i.e. $G_{ij}=G^0_{ij}*G$, with G being the isotropic Green's function of L. We also considered a plastic eigendistortion spread according to

$$\beta^P_{pq}=\beta^{P0}_{pq}*G \tag{22}$$

so that $L\beta^P_{pq}=\beta^{P0}_{pq}$ and $L\alpha_{pq}=\alpha^0_{pq}$. In the isotropic case,[2] this choice yields

$$u_i=\frac{1}{8\pi}\partial_j\Delta R*G*\beta^{P0}_{ij}-U_{ikl}R*G*\alpha^0_{kl}=\frac{1}{8\pi}\partial_j\Delta A*\beta^{P0}_{ij}-U_{ikl}A*\alpha^0_{kl}\quad\text{(Burgers equation)} \tag{23a}$$

$$\sigma_{ij}=S_{ijpq}R*G*\alpha^0_{pq}=S_{ijpq}A*\alpha^0_{pq}\quad\text{(Peach–Koehler stress equation)} \tag{23b}$$

where the function $A(\boldsymbol{x})$ is defined by the convolution $A=R*G$, and satisfies $LA=R$. Because L is isotropic, the function $A(\boldsymbol{x})$ depends only on R. This is expressed as (Lazar, 2012, 2013)

$$A(R)=R*G=R+\frac{2\ell^2}{R}\left(1-e^{-R/\ell}\right) \tag{24}$$

It may further be observed that the solution (23) appears formally similar to (14). However, because the spreading function $A(R)$ arises naturally in the formulation due to the presence of the operator L, the theory does not suffer the limitations discussed in the previous section. To see this, we consider again the Peach–Koehler force exerted on a dislocation using the construction based on the Eshelby stress tensor in gradient elasticity (Lazar and Kirchner, 2007). This yields

$$\begin{aligned}\int_{\mathbb{R}^3}[W\delta_{kj}-(\sigma_{ij}-\ell^2\sigma_{ij,mm})\beta^E_{ik}-\ell^2\sigma_{im,j}\beta^E_{ik,m}]_{,j}\,dV&=\int_{\mathbb{R}^3}\epsilon_{kjm}[\sigma_{ji}\alpha_{im}+\ell^2\sigma_{ij,p}\alpha_{im,p}]\,dV\\&=\int_{\mathbb{R}^3}\epsilon_{kjm}[\sigma_{ji}L\alpha_{im}+(\tau_{ijp}\alpha_{im})_{,p}]\,dV\\&=\int_{\mathbb{R}^3}\epsilon_{kjm}\sigma_{ji}\alpha^0_{im}\,dV=\oint_{\mathcal{L}}\underbrace{\epsilon_{kjm}\sigma_{ji}b_i\,dL_m}_{df_k}\end{aligned} \tag{25}$$

Note that in the third equality we have used the fact that $L\alpha_{im}=\alpha^0_{im}$, and integration by parts was employed to drop terms at infinity. It is therefore shown that, in gradient elasticity of Helmholtz type, the Peach–Koehler force retains its classical form, in the sense that it involves only the Cauchy stress. No other stress measures enter the formulation. In particular, like in the classical case, the stress that appears in the Peach–Koehler force between two dislocation loops is the Peach–Koehler stress (23b).

[2] In gradient elasticity we should distinguish between two types of anisotropy. The first is the anisotropy of the bulk, which is described by the elastic constants c_{ijkl}. The second is the anisotropy of the gradient parameters. In the context of dislocation theory, the latter could be employed to model core anisotropy, but it is likely to introduce significant mathematical complexity in the theory. For additional discussion on this topic see also Lazar and Agiasofitou (2011).

Similarly to the theories analyzed in the previous sections, it is now useful to consider the interaction energy between two dislocation loops. Neglecting surface integrals that vanish at infinity, the interaction energy in gradient elasticity of Helmholtz type can be found as

$$E_I = \int_{\mathbb{R}^3} (\sigma_{ij}^{(1)}\beta_{ij}^{E(2)} + \ell^2\sigma_{ij,m}^{(1)}\beta_{ij,m}^{E(2)})\,dV = \int_{\mathbb{R}^3} \sigma_{ij}^{(1)} L\beta_{ij}^{E(2)}\,dV = \int_{\mathbb{R}^3} \sigma_{ij}^{(1)} L(u_{i,j}^{(2)} - \beta_{ij}^{P(2)})\,dV$$
$$= \int_{\mathbb{R}^3} (L\sigma_{ij}^{(1)} u_{i,j}^{(2)} - \sigma_{ij}^{(1)} L\beta_{ij}^{P(2)})\,dV = -\int_{\mathbb{R}^3} [(L\sigma_{ij}^{(1)})_{,j} u_i^{(2)} + \sigma_{ij}^{(1)} L\beta_{ij}^{P(2)}]\,dV = -\int_{\mathbb{R}^3} \sigma_{ij}^{(1)}\beta_{ij}^{P0(2)}\,dV \tag{26}$$

Using the non-singular Peach–Koehler stress (23b), the following non-singular expression for the interaction energy is obtained:

$$E_I = -\int_{\mathcal{S}^{(2)}} \oint_{\mathcal{L}^{(1)}} S_{ijkl} A(R)\; b_k^{(1)}\, dL_l^{(1)} b_i^{(2)} dA_j^{(2)} = -\oint_{\mathcal{L}^{(2)}} \oint_{\mathcal{L}^{(1)}} M_{ijkl} A(R)\; b_k^{(1)}\, dL_l^{(1)} b_i^{(2)}\, dL_j^{(2)} \tag{27}$$

where M_{ijkl} is the same as in Eq. (11). Eq. (27) is a new result valid for dislocation loops in gradient elasticity of Helmholtz type.

Some remarks are noteworthy. First, that in gradient elasticity of Helmholtz type, all the fundamental equations of dislocation theory (Burgers equation (23a), Peach–Koehler stress (23b), Peach–Koehler force (25), interaction energy equation (27)) are intrinsically non-singular. Second, that all the aforementioned equations retain their classical structure, in the sense that they can simply be obtained from their classical counterparts through the substitution $R(\boldsymbol{x}) \to A(R(\boldsymbol{x}))$. This implies that implementation of the non-singular equations into existing DD codes requires only minimal modification of the integration kernels. Third, we observe that the integration kernels tend rapidly to their classical counterparts and therefore the use of the computationally more expensive[3] non-singular kernels is only necessary when R falls below a few characteristic lengths. For completeness and convenience of implementation, all the fundamental non-singular equations of discrete dislocation theory in gradient elasticity of Helmholtz type are given in component-independent form in Appendix A. We further remark that all the fundamental equations can be expressed as line integrals, which is an essential requirement for DD. In this regard, the conditions under which the generalized solid angle appearing in the Burgers equation (23a) can be expressed as a line integral are discussed in details in Appendix B.

3. Determination of the characteristic parameter ℓ

The gradient formulation introduces the characteristic parameter ℓ, which we estimate here by a matching procedure[4] with the results of atomistic calculations. For this study, tungsten (W) has been selected as the reference isotropic material for our analysis and MS calculations have been performed using the LAMMPS software (Plimpton, 1995). The interatomic potential used was the EAM3 potential described in Cereceda et al. (2013), which was fitted specifically to reproduce dislocation properties in W. Quantities of interest for this potential are lattice parameter $a = 3.1433$ Å, Burgers vector $b = a\sqrt{3}/2$, and shear modulus $\mu = 161$ GPa. To accurately calculate the displacement field of an edge dislocation with minimal end effects, an edge dislocation dipole configuration was implemented in a fully periodic supercell. To do this, an initially perfect lattice was constructed, approximately 720 b in the [111] (Burgers) direction by 1077 b in the $[\bar{1}10]$ direction. In the line direction, the crystal was given the minimum thickness for periodicity, which included six atomic layers of the stacking sequence of the body centered cubic (bcc) structure in the $[\bar{1}\bar{1}2]$ direction, giving a total of approximately 2.85 million atoms in the crystal. The edge dislocations were then generated in a two step procedure. First, all atoms residing within the rectangular region bounded by $[\frac{1}{4}H, \frac{3}{4}H]$ in $[\bar{1}10]$ and $[W-b, W]$ in [111] were removed. Here, H and W represent the total crystal length in the $[\bar{1}10]$ and [111] directions, respectively. Next, all atoms remaining in the region $[\frac{1}{4}H, \frac{3}{4}H]$ in $[\bar{1}10]$ were given displacements linearly ramped from 0 to b, from $[0, W-b]$ in the [111], giving full periodicity in all directions in the crystal and leaving edge dislocations at $(\frac{1}{2}W, \frac{3}{4}H)$ and $(\frac{1}{2}W, \frac{1}{4}H)$. Molecular statics calculations were then performed using the conjugate gradient minimization scheme which terminated when a stopping criteria was met. The criteria was chosen as an energy change of less than several thousandths of an eV per atom in the crystal per minimization step. In cases where the initial configuration was very close to a local (and not global) energy minimum, all atomic positions were slightly randomly perturbed to assist the minimization in locating the global minimum. Atomic stresses were computed using the virial formulation built into LAMMPS.

To extract the characteristic parameter, ℓ, a post-processing algorithm was written to apply the continuum stress field described by (A.12), to a representative lattice identical to the pre-relaxed crystal used in the atomistic calculations. Using ℓ as a fitting parameter, the stress components of rows of atoms in the [111] and $[\bar{1}10]$ directions near the dislocation core were directly compared to the atomistic results, and the best value of ℓ was obtained through a minimization of the residual. Results of the fitting procedure are shown in Fig. 1. For the potential considered, the best fitting value was $\ell = 0.85b$. Similar calculations were also performed for a screw dislocation in W. However, the sparsity of the atoms on the (111) plane does not allow to resolve the rise, saddle point and inflection of the stress components near the core, hence resulting in a less rigorous

[3] For example, in our implementation, the computation of the stress kernel of Eq. (A.12) is about 40% slower than the corresponding classical kernel.

[4] We remark that the fitting procedure described in this section should not be interpreted as an attempt to describe the core structure of the material, which is outside the scope of linear elasticity, but simply as a possible method to estimate the value of the characteristic length ℓ.

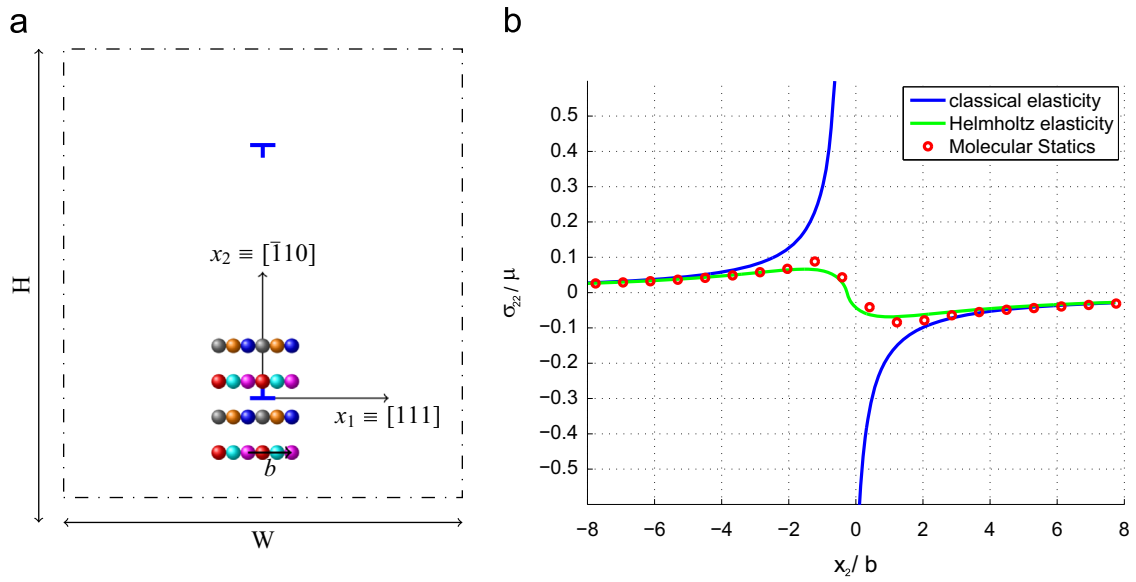

Fig. 1. Stress field in the vicinity of an edge dislocation in W: comparison between analytical and MS results. (a) A dislocation dipole in the shown orientation is introduced into a perfect bcc tungsten lattice and given full periodicity. In the figure, atoms (represented by spheres) of the same color are co-planar normal to the line direction. The modified lattice is relaxed using conjugate gradient molecular statics calculations to find the minimum energy configuration, and the characteristic length parameter extracted. (b) The stress component σ_{22} obtained in MS in the relaxed configuration, plotted as a function of the reference coordinate x_2, and compared to the gradient and classical elasticity solutions. The gradient solution is plotted using a gradient parameter $\ell = 0.85b$. (For interpretation of the references to color in this figure caption, the reader is referred to the web version of this article.)

fitting procedure for ℓ. Therefore, in first approximation, the value of ℓ found for an edge dislocation is applied for the entire loop.

4. Applications

4.1. Displacement field around a dislocation loop

As a first application of the non-singular gradient theory of discrete dislocation loops, we wish to analyze the displacement discontinuity across the slip plane of a dislocation loop and discuss important consequences related to it. In the case of a Volterra dislocation, the displacement field of a dislocation loop which bounds a surface $\mathcal{S}$ suffers a constant jump discontinuity $\boldsymbol{b}$ (Burgers vector) across $\mathcal{S}$. From the viewpoint adopted in this paper, the discontinuity is caused by the fact that the plastic distortion $\boldsymbol{\beta}^{P0}$ is concentrated on $\mathcal{S}$ according to Eq. (5). The displacement jump is manifest in the discontinuity of the solid angle Ω^0 present in the first term of Eq. (7a). Clearly, a constant displacement jump is not physical for a crystal dislocation, because it would require either creation of gaps or interpenetration of matter, and the classical theory breaks down at the dislocation core.

In view of the previous considerations, it is interesting to understand how the non-singular gradient theory of discrete dislocations overcomes the fundamental difficulties of the classical theory of Volterra dislocations. The key observation is that the gradient solution assumes a plastic distortion, which is not concentrated on the slip surface, but instead is distributed in the volume around $\mathcal{S}$ according to Eq. (22). As a consequence, the displacement field (23a) involves a generalized solid angle $\Omega = \Omega^0 * G$, which regularizes the classical Volterra discontinuity. The concept of generalized solid angle and its surface and line integral representations are discussed in details in Appendix B. Here we simply remark that the displacement field is continuous on the slip plane and the "jump" $\boldsymbol{b}$ results distributed in the volume around the slip plane. The size of the distorted region clearly depends on the characteristic length scale ℓ.

The fundamental difference between classical and gradient theories of dislocations is illustrated in Fig. 2, where we plot the component of displacement associated with the solid angle for both the classical and the gradient theory. In particular, we consider a circular loop of radius R and two points, A and B located across the slip plane at a distance h from it, and both at the same distance r from the loop axis. We plot the difference Δu in their displacement field, which depends both on r and on the height h from the slip plane, that is $\Delta u(r,h) = u(A) - u(B)$. From Fig. 2(b), one can see that the gradient theory predicts that $\Delta u(r,h)$ is zero on the slip plane ($h=0$), and therefore there is no displacement discontinuity across the slip plane. This contrasts the classical result, where the slip plane experiences a displacement discontinuity equal to b inside the loop ($r < R$), and zero outside ($r > R$). Outside the slip plane, i.e. for $h > 0$, $\Delta u(r,h)$ approaches its classical counterpart. However an important observation can be made: for small h, the displacement field predicted by the gradient solution increases gradually from zero, while the classical theory predicts values close to b. This fact has significant physical consequences. Consider for example the energetics of face centered cubic (fcc) crystals, where a Shockley partial dislocation loop encloses a stacking fault with energy density γ per unit slip area. The quantity γ must be interpreted as the generalized

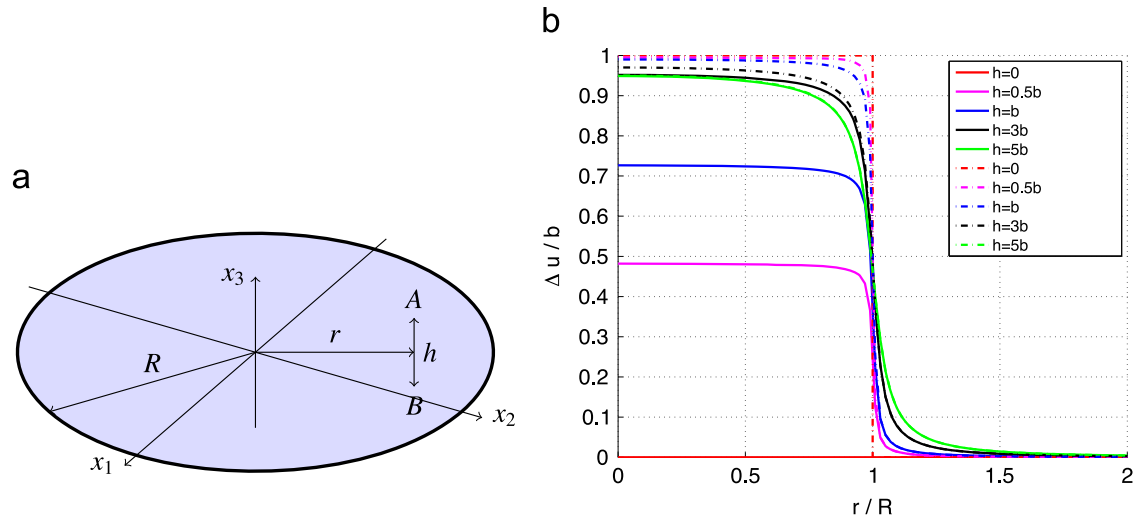

Fig. 2. Component of displacement associated with the solid angle of a dislocation loop. (a) Points A and B are positioned across the slip plane of a circular dislocation loop of radius R, both at a distance r from the loop axis and separated by a distance h. The quantity $\Delta u(r,h)=u(A)-u(B)$ is the difference in the component of displacement along the Burgers vector between the two points. (b) Function $\Delta u(r,h)$ for different values of h for a loop radius $R=100b$, and a typical characteristic length $\ell=b$. Comparison between classical Volterra (dashed lines) and Helmholtz gradient elasticity. Notice that, for $h=0$, the classical solution predicts a discontinuity, while the gradient solution is always continuous. Moreover, for small h, the classical theory predicts that $\Delta u\approx b$, while, for the gradient theory, Δu remains a small fraction of b.

stacking fault energy density because it depends on the relative displacement Δu between the two atomic layers across the slip plane. In the classical case, this displacement is approximately constant and equal to the magnitude b_p of the partial Burgers vector. Therefore $\gamma(\Delta u)=\gamma(b_p)=\gamma_i$ is also constant and equal to the intrinsic stacking fault energy density of the material. The total stacking fault is then simply $\pi R^2\gamma_i$. On the other hand, according to the gradient theory, the difference Δu between atomic layers varies gradually about the slip plane together with the stacking fault energy density. Implications of this observation are discussed in details in the following section.

4.2. Applications to homogeneous dislocation nucleation

A well-known issue in computational DD is the lack of a simple continuum criterion of dislocation nucleation that can be used during simulations to inject new dislocations into the simulation volume. Although in samples of sub micron finite volume, the rate of dislocation nucleation is likely to be controlled by emission from the crystal surface, here we consider the case of homogeneous nucleation in bulk crystals (e.g. in shock compression above the Hugoniot elastic limit). A simple elastic model of homogeneous nucleation of a shear loop is described by Hirth and Lothe (1992) (ch. 20-5). The model assumes that nucleation of a circular dislocation loop is a thermally assisted process having a rate that is proportional to the probability of success of a thermal fluctuation, $\exp(-\Delta G^*(\tau)/kT)$. Here $\Delta G^*(\tau)$ is the nucleation barrier as a function of the applied stress, that is the maximum of the following Gibbs free energy with respect to the loop radius R:

$$\Delta G(R,\tau)=E_e(R)-W(R,\tau)+E_m(R)=E_e(R)-\pi R^2 b\tau+\pi R^2\gamma_i \tag{28}$$

In Eq. (28), the free energy of nucleation comprises the elastic energy $E_e(R)$ of the loop, the work done by a (constant) external shear stress τ in expanding the loop, and a misfit energy E_m. For fcc crystals, the misfit energy needs to be accounted for because the nucleation of a partial dislocation loop gives rise to a stacking fault with energy density γ per unit area. As mentioned in the previous section, according to the classical theory, γ can be considered constant and equal to the intrinsic stacking fault energy γ_i of the material. As a consequence, the total misfit energy of the stacking fault is simply $\pi R^2\gamma_i$.

The physical reason corresponding to the request that ΔG be maximum has an obvious interpretation in terms of forces per unit line of dislocation. In fact, vanishing the derivative of (28) with respect to the loop radius and dividing by $2\pi R$, one finds that the maximum of ΔG corresponds to the condition:

$$b\tau-\frac{1}{2\pi R}\frac{dE_e}{dR}-\gamma_i=f_{ext}+f_{self}+f_\gamma=0 \tag{29}$$

This result simply means that the loop becomes unstable when the applied radial force per unit length $b\tau$ overcomes the sum of the self force per unit length $-1/(2\pi R)\,dE_e/dR$ and the lattice force per unit length $-\gamma_i$ which both tend to collapse the loop. Aubry et al. (2011) have compared different versions of the classical nucleation model to nudged elastic band atomistic calculations. It was shown that the classical model is not in good agreement with the atomistic results even if the cut-off radius used to compute the elastic energy is chosen as a fitting parameter, and the atomistic results could be reproduced only when the influence of stress on the stacking fault energy was taken into account.

Here we wish to apply the gradient theory of dislocation loops to the nucleation model of Hirth and Lothe (1992) for fcc metals. The use of the gradient theory implies two main modifications of the classical model. First, the elastic energy term in

Eq. (28) is computed as 1/2 of the non-singular interaction energy between the loop and itself, that is as 1/2 of the expression given in (27). Second, that stacking fault energy density γ is not assumed to be constant but dependent on the difference in displacement between the two layers of atoms immediately across the slip plane. This difference is measured by the function Δu plotted in Fig. 2(b) for h equal to the distance between (111) planes in fcc metals. With these modifications the nucleation barrier is the maximum of the following free energy:

$$\Delta G(R,\tau) = \tfrac{1}{2} E_I(R) - \pi R^2 b\tau + \int_0^\infty 2\pi r \gamma(\Delta u(r,R))\, dr \tag{30}$$

The function $\Delta G(R,\tau)$ is constructed numerically in the range $0 \le R \le 15 b_p$ using our DD code (Po et al., 2013). For each discrete value of R, the following computer simulation is performed. The circular loop is discretized in a number of segments proportional to the loop radius in order to maintain good numerical convergence. Each segment is parametrized by a cubic spline so that tangent continuity is maintained across segments. With this discretization, Eq. (27) is integrated numerically using 32 quadrature points per segment. The elastic energy computed according to this procedure is then summed to the work done by the stress field τ and to the misfit energy in order to form the Gibbs energy of activation according to (30). The material of choice is Cu and the function $\gamma(\Delta u)$ is taken from Aubry et al. (2011). The displacement $\Delta u(r,R)$ is computed as shown in the previous section as a function of both r and R, for h equal to the distance between (111) planes in fcc crystals, that is $h = b\sqrt{(6)}/3 = b_p\sqrt{(2)}$, where b_p is the magnitude of the Shockley partial dislocation.

Results of our calculations are shown in Fig. 3. In particular, the function $\Delta G(R,\tau)$ is shown in Fig. 3(a) for different values of the applied stress τ, and compared to the corresponding quantity computed according to the classical model (model I in

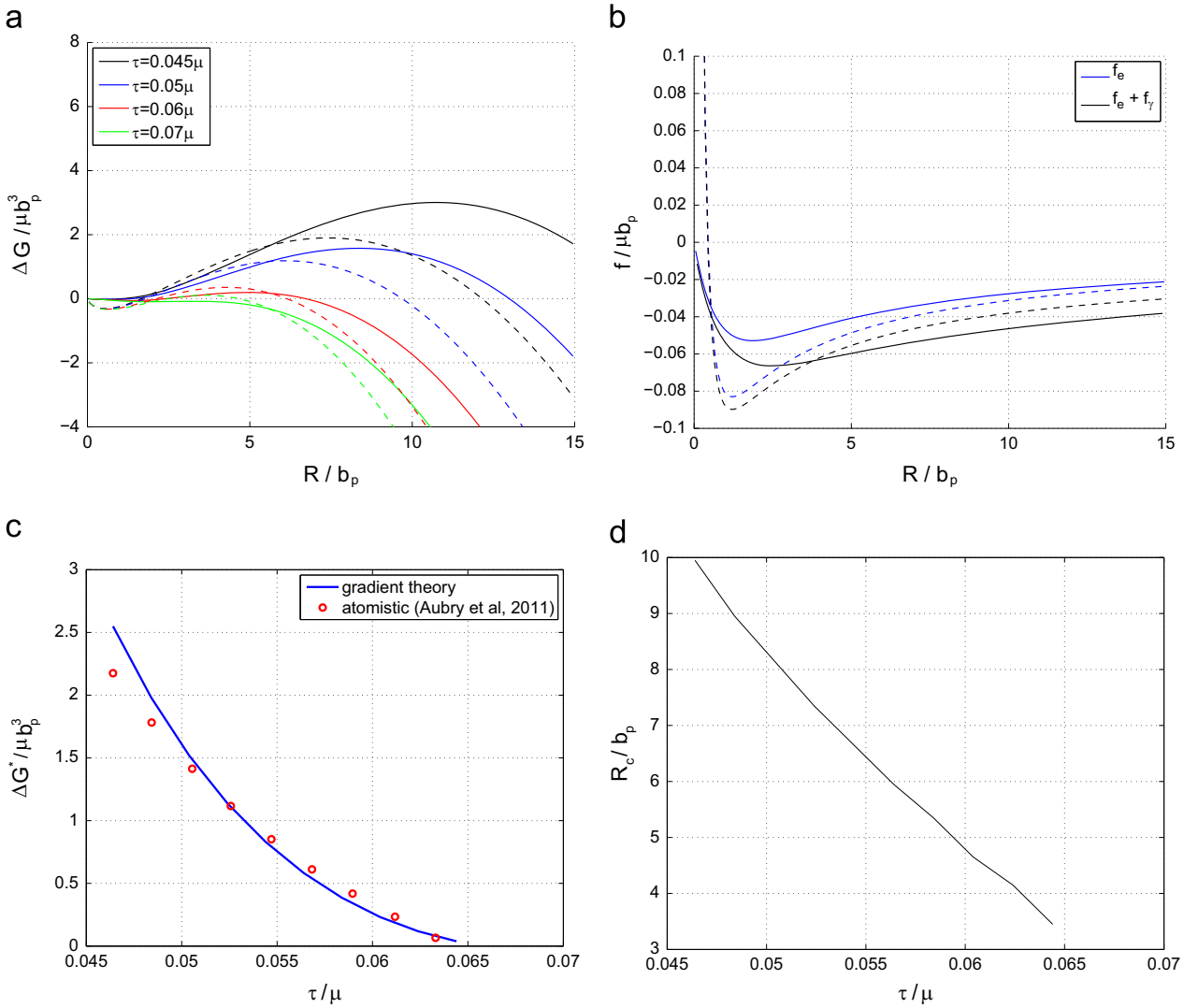

Fig. 3. (a) Free energy of nucleation as a function of the loop radius at various applied stresses. Solid lines represent the gradient elasticity solution using a characteristic parameter $\ell = 1.2 b_p$, while dashed lines correspond to the classical model (model I in Aubry et al., 2011). (b) Self-elastic force per unit length $f_e = -1/2\pi R\, dE_e/dR$ and force due to the stacking fault $f_\gamma = -1/2\pi R\, dE_m/dR$: gradient elasticity (solid lines) vs classical model. (c) Nucleation barrier computing according as $\Delta G^*(\tau) = \max \Delta G(R,\tau) - \min \Delta G(R,\tau)$, with $\Delta G(R,\tau)$ from (a). Comparison with the atomistic results of Aubry et al. (2011). (d) Critical radius of nucleation as a function of the applied stress.

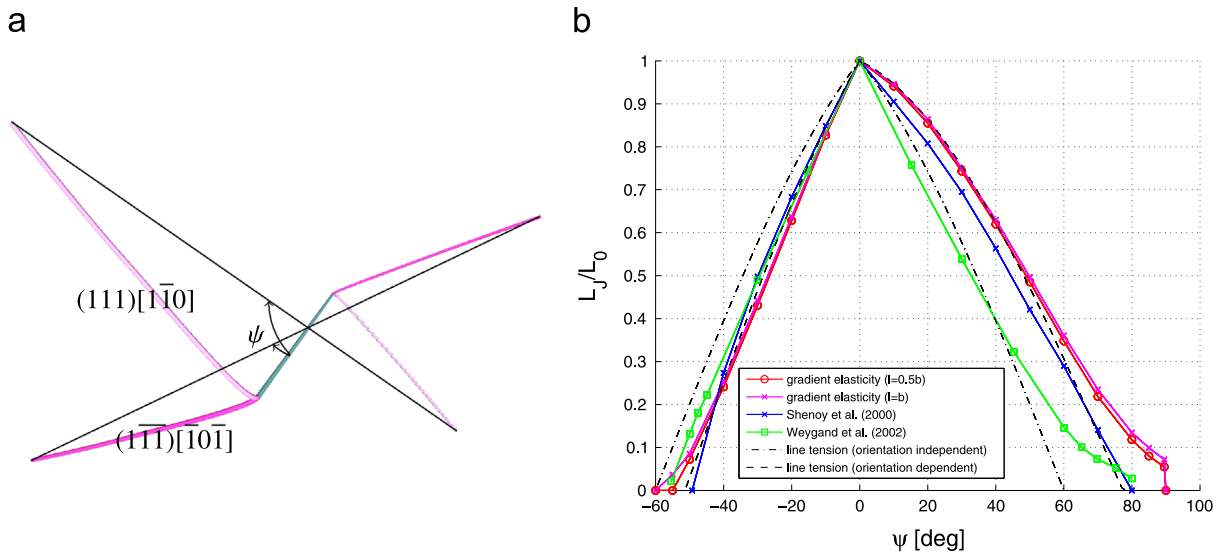

Fig. 4. Strength of Lomer–Cottrell junctions in Al. (a) Lomer–Cottrell junction that forms between a (111)[1$\bar{1}$0] dislocation and a (1$\bar{1}\bar{1}$)[$\bar{1}$0$\bar{1}$]. In the initial configuration (black line), each dislocation has a length L_0, it is pinned at the end points, and forms an angle ψ with the [0$\bar{1}$1] direction. Colors represent different Burgers vectors. (b) Length of the junction segment as a function of the angle ψ. (For interpretation of the references to color in this figure caption, the reader is referred to the web version of this article.)

Aubry et al., 2011). It can be noticed that, for each τ, $\Delta G(R,\tau)$ shows a minimum and a maximum value. Beltz and Freund (1993) have suggested that the difference between the maximum and minimum values, rather than the maximum, be taken for the nucleation energy barrier, $\Delta G^*(\tau)$ at fixed τ. Following this interpretation, we plot $\Delta G^*(\tau)$ in Fig. 3(c). A comparison of gradient elasticity results with the atomistic calculations of Aubry et al. (2011) is also presented. The critical radius at nucleation $R_c(\tau)$ corresponding $\Delta G^*(\tau)$ is shown in Fig. 3(d). We also plot the results of our calculations in terms of forces per unit line of dislocation. Fig. 3(b) shows the contributions of the self-elastic force of the loop and of the force due to the stacking fault. It is seen that the total self-force attempting to shrink the loop (elastic plus stacking fault contributions) admits a minimum corresponding to a critical stress $\tau_c \approx 0.065\mu$. Clearly, we have $\Delta G^*(\tau_c)=0$ and thereforeτ_c is the stress of athermal dislocation nucleation. The existence of a minimum implies that any external stress larger than $\tau_c > 0$ exerts an expanding force on the loop that cannot be balanced by the total self force. Therefore the stress of athermal nucleation can be considered the shearing strength of the crystal predicted by the present non-singular gradient theory.

4.3. Strength of dislocation junctions

One of the main limitations of current DD models is the inability to resolve dislocation interactions in close range without ad-hoc regularization strategies, such as the use of cut-off radii, the regularization technique (Brown, 1964), or the line-tension approximation. The regularization offered by the gradient theory is particularly advantageous for DD simulations involving the formation of junctions between dislocations, because it removes the issue of divergent stress field caused by intersecting dislocation segments. In order to understand the sensitiveness of the junction strength predicted by gradient theory on the characteristic parameter ℓ, here we perform a series of simple DD simulations to compute the strength of a Lomer–Cottrell junction in fcc metals, and compare our results to similar data found in the literature. With reference to Fig. 4(a), we consider the Lomer–Cottrell junction that forms between a (111)[1$\bar{1}$0] dislocation and a (1$\bar{1}\bar{1}$)[$\bar{1}$0$\bar{1}$] dislocation. Each dislocation, originally straight, is supposed to be pinned at its end points. The distance between the end points is $L_0 = 200b$, and the angle that each dislocation forms with the [0$\bar{1}$1] is ψ. The material of choice is Al, a fcc metal with high stacking fault energy, so that the disassociation in partials can be neglected. DD simulations are performed to relax the initial configuration. In the final state, the length L_j of the junction segment that forms along the [0$\bar{1}$1] direction is measured as a function of ψ. The plot of $L_J(\psi)$ is shown in Fig. 4(b) and compared to similar results obtained by other nodal DD simulations based on the Brown (1964) cut-off procedure: the partial dislocation model of Shenoy et al. (2000) and the full dislocation model of Weygand (2002). We also show the prediction of orientation independent and orientation dependent line tension analytical models (Wickham et al., 1999; Shin et al., 2001; Dupuy and Fivel, 2002). Our results are in good agreement with the orientation-dependent line tension model in the range $-40 \le \psi \le 60$. Outside this range, the effects of the dislocation curvature captured by the DD simulation and neglected by the line tension model become evident. Moreover, the final configuration of stronger junctions is dominated by long-range interactions and therefore the results are largely independent of the parameter ℓ. The influence of the parameter ℓ, which affects the local force equilibrium at the triple points, starts to appear only for weaker junctions. This simple result suggests that the macroscopic hardening characteristics obtained by DD simulations, which are expected to be governed by strong junctions,

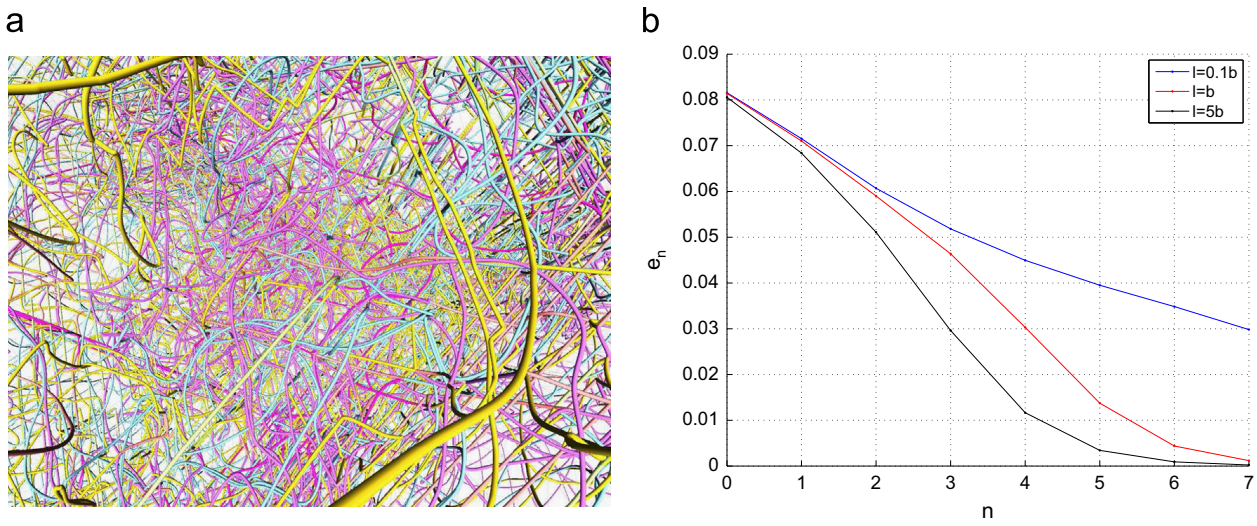

Fig. 5. Numerical convergence of the nodal force vector in DD simulations for different values of the characteristic parameter ℓ. (a) The dislocation network in a Cu cube of side length 5μ used for the calculation of the nodal force vector. This configuration includes various structures such as junctions, cross slips and jogs. The dislocation network is discretized in segments parametrized by cubic splines and, for each segment, the number of quadrature points is chosen so that the distance between them is $\Delta L_n \approx b2^{8-n}$. For each n, a nodal force vector $\boldsymbol{F}_n$ is computed. (b) Plot of $e_n = \|\boldsymbol{F}_{n+1} - \boldsymbol{F}_n\| / \|\boldsymbol{F}_n\|$ vs n for different values of the characteristic parameter ℓ.

will be insensitive to small uncertainties in the choice of the characteristic length scale parameter ℓ. It also confirms the well-known classical result that the contribution of the dislocation core region to junction stability is negligible compared to the elastic contribution from regions outside the core (e.g. Madec et al., 2002).

4.4. Numerical convergence of DD simulations with gradient elasticity

We now turn our attention to the study of numerical convergence related to the implementation of the gradient theory of discrete dislocation loops in DD simulations. To this end, we recall that, in DD, the law governing the motion of dislocation loops is usually taken in the form:

$$B\boldsymbol{v} = \boldsymbol{f} \tag{31}$$

where, B is an effective drag coefficient, $\boldsymbol{v}$ is the local dislocation velocity, and $\boldsymbol{f}$ is the local Peach–Koehler force on the dislocation line. In the nodal DD approach, Eq. (32) is solved in a weak sense (Ghoniem et al., 2000). In fact, upon discretization of the dislocation network in a finite set of interconnected dislocation segments, it corresponds to a matrix equation of the type:

$$\mathbb{B}\boldsymbol{V} = \boldsymbol{F} \tag{32}$$

where $\mathbb{B}$ is the "stiffness" matrix of the dislocation network, $\boldsymbol{V}$ is the global vector of nodal dislocation velocities, and $\boldsymbol{F}$ is the global nodal force vector. From a numerical viewpoint, computation of the matrix $\mathbb{B}$ does not pose particular challenges. On the other hand, the nodal force vector $\boldsymbol{F}$ requires integration of the non-singular but possibly rapidly varying Peach–Koehler force along the dislocation line (see Po and Ghoniem, 2014, for details). In our implementation, numerical integration is performed using a certain number of quadrature points per dislocation segment, chosen in a way that quadrature points are uniformly spaced at a distance $\Delta L_n \approx b2^{8-n}$, for non-negative integer n. For each n we let $\boldsymbol{F}_n$ be the corresponding numerical value of the nodal force. The relative error between integration schemes of consecutive order can be measured by the sequence:

$$e_n = \frac{\|\boldsymbol{F}_{n+1} - \boldsymbol{F}_n\|}{\|\boldsymbol{F}_n\|} \tag{33}$$

In order to study the sensitiveness of e_n to the choice of the gradient parameter ℓ, we consider a dislocation configuration obtained in a typical DD simulation in Cu. The dislocation network in this configuration occupies a cubic volume of side length 5μ and, as shown in shown in Fig. 5(a), it contains a rich variety of dislocation structures including junctions, cross-slips and jogs. The dislocation network is discretized into segments parametrized by cubic spines so that the tangent continuity at the dislocation nodes is preserved. For this configuration, the nodal force vector $\boldsymbol{F}_n$ including only the force contribution of the mutual dislocation interaction is computed for different values n and plotted in Fig. 5(b). As expected, the convergence of e_n is more rapid for larger values of the characteristic parameter ℓ, which correspond to smoother stress fields near dislocation cores. For a realistic value of ℓ, such as $\ell = b$, a spacing $\Delta L \approx 32b$ guarantees numerical error on the order of 5%. Finally we remark that, in the presence of an external stress, the error estimate found here becomes an upper

bound of the true error, and that the error in force calculations can be made arbitrarily small by increasing number of quadrature points at the expense of computational speed.

5. Summary and conclusions

In this paper, we discussed theoretical and computational aspects of the non-singular theory of discrete dislocation loops in gradient elasticity of Helmholtz type, with interest in its application to three-dimensional DD simulations. The theory has been presented in the general framework of linearized incompatible elasticity with plastic eigenstrains. This allowed us to establish differences and analogies between the present gradient theory, the classical theory, and the non-singular theory developed by Cai et al. (2006). The unified framework used in the first part of the paper has also allowed us to obtain new results by extending the corresponding concepts in classical elasticity. First, we derived the non-singular expression for the interaction energy between two dislocation loops in gradient elasticity of Helmholtz type. This is a fundamental equation that can be used to compute the self-energy of an arbitrary loop without the use of the line tension approximation. Second, the Eshelby (1982)–de Wit (1981) line integral transformation of the solid angle associated with the displacement field of a dislocation loop has been extended to the case of dislocations with a spread core. In Appendix B, it is found that the conditions under which a line integral representation of the solid angle exists are more restrictive than the case of classical elasticity, but are still applicable to DD simulations. With these new results, all the fundamental equations of dislocation theory in gradient elasticity of Helmholtz type can be expressed as non-singular line integrals. This is a fundamental requirement for application of the theory to DD simulations. These equations are given in component-independent form in Appendix A. Remarkably, we observe that all the fundamental equations of dislocation theory can be obtained from their classical counterparts with the substitution $R \to A(R)$. As a consequence, not only the gradient theory provides a regularization of all the classical singularities associated with the fields of discrete dislocation loops, but also its implementation in existing DD results extremely simple and numerically efficient. The benefits of the theory come at a small price, which is the need to identify the value of the only characteristic length scale parameter ℓ. Although several identification techniques may exist, we have proposed that the gradient parameter be found by comparison between the dislocation stress field predicted by the theory and results obtained from atomistic MS simulations.

Significant consequences and applications of the gradient theory of discrete dislocations to DD simulations have been considered in Section 4. The present implementation of the eigenstrain gradient elasticity theory of dislocations shows results of near atomic precision and resolves a major impediment in DD simulations that are based on classical Volterra dislocations. Consistent with atomistic calculations, we find that the displacement field around a dislocation loop is smooth, and that the loop self-energy is non-divergent. With these results the energy barrier of nucleation of a circular loop is shown to be in good agreement with atomistic calculations. DD simulations of Lomer–Cottrell junctions in Al show that the strength of the junction and its configuration are easily obtained, without ad-hoc regularization of the singular field. For a typical dislocation network in Cu, DD simulations show that the error in the mutual interaction forces between dislocation segments can be arbitrarily reduced, and that for typical values of the characteristic length scale parameter $\ell \approx b$, it is estimated to be less than $< 5\%$ using a distance of $\approx 32\ b$ between quadrature points.

Acknowledgments

Giacomo Po, Dariush Seif, and Nasr Ghoniem wish to acknowledge the support of the Air Force Office of Scientific Research (AFOSR), through award No: FA9550-11-1-0282 with UCLA. Markus Lazar gratefully acknowledges the grants obtained from the Deutsche Forschungsgemeinschaft (Grant nos. La1974/2-1, La1974/2-2, La1974/3-1).

Appendix A. Elastic fields of dislocations loops in gradient elasticity of Helmholtz type: component-independent form

In order to derive the component-independent form of the fundamental equations of dislocation theory in gradient elasticity of Helmholtz type, it is convenient to introduce the following differential operators:

$$F_1 = \Delta \quad F_2 = \frac{1}{R}\frac{\partial}{\partial R} \quad F_3 = F_1 - 3F_2 \tag{A.1}$$

$$F_4 = \frac{\partial}{\partial R}\Delta \quad F_5 = \frac{1}{R}F_3 \quad F_6 = F_4 - 5F_5 \quad F_7 = F_5 - F_4 \tag{A.2}$$

When applied to the function $A(R,\ell)$, given in Eq. (24), these operators generate the following scalar functions:

$$f_1(R,\ell) = F_1[A(R,\ell)] = \Delta A(R,\ell) = \frac{2}{\ell} f_1^*(R/\ell) \quad f_1^*(x) = \frac{1-e^{-x}}{x} \tag{A.3}$$

$$f_2(R,\ell) = F_2[A(R,\ell)] = \frac{1}{R}\frac{\partial A(R,\ell)}{\partial R} = \frac{2}{\ell} f_2^*(R/\ell) \quad f_2^*(x) = \frac{\frac{1}{2}x^2 + (1+x)e^{-x} - 1}{x^3} \tag{A.4}$$

$$f_3(R,\ell)=F_3[A(R,\ell)]=\frac{2}{\ell}f_3^*(x)\quad f_3^*(x)=f_1^*(x)-3f_2^*(x) \tag{A.5}$$

$$f_4(R,\ell)=F_4[A(R,\ell)]=\frac{\partial}{\partial R}\Delta A(R,\ell)=\frac{2}{\ell^2}f_4^*(R/\ell)\quad f_4^*(x)=\frac{df_1^*(x)}{dx}=\frac{(1+x)e^{-x}-1}{x^2} \tag{A.6}$$

$$f_5(R,\ell)=F_5[A(R,\ell)]=\frac{2}{\ell^2}f_5^*(R/\ell)\quad f_5^*(x)=\frac{f_3^*(x)}{x} \tag{A.7}$$

$$f_6(R,\ell)=F_6[A(R,\ell)]=\frac{2}{\ell^2}f_6^*(R/\ell)\quad f_6^*(x)=f_4^*(x)-5f_5^*(x) \tag{A.8}$$

$$f_7(R,\ell)=F_7[A(R,\ell)]=\frac{2}{\ell^2}f_7^*(R/\ell)\quad f_7^*(x)=f_5^*(x)-f_4^*(x) \tag{A.9}$$

The component-independent forms of the fundamental equations of dislocation theory in gradient elasticity of Helmholtz type are now derived using the functions $f_1^*\ldots f_7^*$.

1. The non-singular displacement field is given by the Burgers equation (23a) in terms of the operator U_{ikl} defined in Eq. (8). Using the chain rule of differentiation, this operator can identically be written in terms of the operators F_1, F_2, and F_3:

$$U_{ikl}=\frac{1}{8\pi(1-\nu)}\Big\{[(1-\nu)F_1-F_2]\epsilon_{ikl}-\hat{R}_i\hat{R}_m\epsilon_{mkl}F_3\Big\} \tag{A.10}$$

Therefore, the component-independent form of (23a) becomes:

$$\boldsymbol{u}(\boldsymbol{x})=-\frac{\boldsymbol{b}\Omega}{4\pi}-\frac{1}{4\pi(1-\nu)\ell}\oint_{\mathcal{L}}\Big\{[(1-\nu)f_1^*(R/\ell)-f_2^*(R/\ell)]\boldsymbol{b}\times\hat{\boldsymbol{\xi}}'-\Big[\hat{\boldsymbol{R}}\cdot\Big(\boldsymbol{b}\times\hat{\boldsymbol{\xi}}'\Big)\Big]\hat{\boldsymbol{R}}f_3^*(R/\ell)\Big\}dL' \tag{A.11}$$

In the previous equation, the symbol $\hat{\boldsymbol{\xi}}$ indicates the unit vector tangent to the dislocation line, $\boldsymbol{R}=\boldsymbol{x}-\boldsymbol{x}'$, $R=\sqrt{\boldsymbol{R}\cdot\boldsymbol{R}}$, and $\hat{\boldsymbol{R}}=\boldsymbol{R}/R$. Under particular conditions, the generalized solid angle Ω can be transformed into a line integral, as discussed in Appendix B.

2. The non-singular Cauchy stress is given by the Peach-Koehler equation (23b) in terms of the operator S_{ijkl} defined in Eq. (8). Using the chain rule of differentiation, this operator can identically be written in terms of the operators F_4, F_5, F_6, and F_7:

$$S_{ijkl}=\frac{\mu}{4\pi(1-\nu)}\left[\frac{1-\nu}{2}(\delta_{il}\epsilon_{jmk}+\delta_{jl}\epsilon_{imk})\hat{R}_mF_4+\Big(\epsilon_{ikl}\hat{R}_j+\epsilon_{jkl}\hat{R}_i\Big)F_5+\epsilon_{klm}\hat{R}_m\Big(\hat{R}_i\hat{R}_jF_6+\delta_{ij}F_7\Big)\right] \tag{A.12}$$

Therefore the component-independent form of (23b) becomes:

$$\begin{aligned}\boldsymbol{\sigma}(\boldsymbol{x})=\frac{\mu}{2\pi(1-\nu)\ell^2}\oint_{\mathcal{L}}\Big\{&\frac{1-\nu}{2}\Big[\hat{\boldsymbol{\xi}}'\otimes\Big(\hat{\boldsymbol{R}}\times\boldsymbol{b}\Big)+\Big(\hat{\boldsymbol{R}}\times\boldsymbol{b}\Big)\otimes\hat{\boldsymbol{\xi}}'\Big]f_4^*(R/\ell)+\Big[\Big(\boldsymbol{b}\times\hat{\boldsymbol{\xi}}'\Big)\otimes\hat{\boldsymbol{R}}+\hat{\boldsymbol{R}}\otimes\Big(\boldsymbol{b}\times\hat{\boldsymbol{\xi}}'\Big)\Big]f_5(R/\ell)\\&+\hat{\boldsymbol{R}}\cdot(\boldsymbol{b}\times\hat{\boldsymbol{\xi}}')[\hat{\boldsymbol{R}}\otimes\hat{\boldsymbol{R}}f_6(R/\ell)+\boldsymbol{I}f_7(R/\ell)]\Big\}dL'\end{aligned} \tag{A.13}$$

3. The non-singular interaction energy between two dislocation loops is given in Eq. (27) in terms of the operator M_{ijkl} defined in Eq. (11). Using the chain rule of differentiation, this operator can identically be written in terms of the operators F_1, F_2, and F_3:

$$M_{ijkl}=\frac{\mu}{4\pi(1-\nu)}\left\{\left(\frac{1-\nu}{2}\delta_{ij}\delta_{kl}+\nu\delta_{il}\delta_{jk}-\delta_{jl}\delta_{ik}\right)F_1+\delta_{jl}\Big[\delta_{ik}F_2+\hat{R}_i\hat{R}_kF_3\Big]\right\} \tag{A.14}$$

Therefore, the component-independent form of (27) becomes:

$$\begin{aligned}E_I=-\frac{\mu}{2\pi(1-\nu)\ell}\oint_{\mathcal{L}_2}\oint_{\mathcal{L}_1}\Big\{&\Big[\frac{1-\nu}{2}\Big(\boldsymbol{b}_1\cdot\hat{\boldsymbol{\xi}}_1\Big)\Big(\boldsymbol{b}_2\cdot\hat{\boldsymbol{\xi}}_2\Big)+\nu\Big(\boldsymbol{b}_1\cdot\hat{\boldsymbol{\xi}}_2\Big)\Big(\boldsymbol{b}_2\cdot\hat{\boldsymbol{\xi}}_1\Big)-(\boldsymbol{b}_1\cdot\boldsymbol{b}_2)\Big(\hat{\boldsymbol{\xi}}_1\cdot\hat{\boldsymbol{\xi}}_2\Big)\Big]f_1^*(R/\ell)\\&+(\hat{\boldsymbol{\xi}}_1\cdot\hat{\boldsymbol{\xi}}_2)[(\boldsymbol{b}_1\cdot\boldsymbol{b}_2)f_2^*(R/\ell)+(\boldsymbol{b}_1\cdot\hat{\boldsymbol{R}})(\boldsymbol{b}_2\cdot\hat{\boldsymbol{R}})f_3^*(R/\ell)]\Big\}dL_1dL_2\end{aligned} \tag{A.15}$$

Notice that the self energy of a loop is 1/2 of the previous expression when the two loops coincide.

4. As shown in equation (25), the Peach-Koehler force per unit line of dislocation is:

$$\boldsymbol{f}=(\boldsymbol{\sigma}\cdot\boldsymbol{b})\times\hat{\boldsymbol{\xi}} \tag{A.16}$$

where $\boldsymbol{\sigma}$ is the Cauchy stress. Therefore, the Peach-Koehler force maintains its classical form.

Finally, notice that the fundamental equations of dislocation theory are expressed in terms of the functions $f_1^*(R/\ell)\ldots f_7^*(R/\ell)$, which are non-singular as their arguments tend to zero. In fact one can easily verify the following limits:

$$\lim_{x\to 0} f_1^*(x)=1 \qquad \lim_{x\to 0} f_2^*(x)=\frac{1}{3} \qquad \lim_{x\to 0} f_3^*(x)=0$$
$$\lim_{x\to 0} f_4^*(x)=-\frac{1}{2} \qquad \lim_{x\to 0} f_5^*(x)=-\frac{1}{8} \qquad \lim_{x\to 0} f_6^*(x)=\frac{1}{8} \qquad \lim_{x\to 0} f_7^*(x)=\frac{3}{8} \tag{A.17}$$

Moreover, it is noteworthy that, for $R\gg\ell$, eqs. (A.11), (A.13), and (A.15) tend to their corresponding classical expressions (e.g. de Wit, 1960). This can be verified considering the following limits:

$$\lim_{R/\ell\to\infty} \frac{f_1^*(R/\ell)}{\ell}=\frac{1}{R} \qquad \lim_{R/\ell\to\infty} \frac{f_2^*(R/\ell)}{\ell}=\frac{1}{2R} \qquad \lim_{R/\ell\to\infty} \frac{f_3^*(R/\ell)}{\ell}=-\frac{1}{2R}$$
$$\lim_{R/\ell\to\infty} \frac{f_4^*(R/\ell)}{\ell^2}=-\frac{1}{R^2} \qquad \lim_{R/\ell\to\infty} \frac{f_5^*(R/\ell)}{\ell^2}=-\frac{1}{2R^2} \qquad \lim_{R/\ell\to\infty} \frac{f_6^*(R/\ell)}{\ell^2}=\frac{3}{2R^2} \qquad \lim_{R/\ell\to\infty} \frac{f_7^*(R/\ell)}{\ell^2}=\frac{1}{2R^2} \tag{A.18}$$

Appendix B. Generalized solid angle for dislocation loops with a spread core: surface and line integral forms

The three dislocation theories considered in this paper predict that the displacement field induced by a dislocation loop in an isotropic medium can be written in the following general form:

$$u_i=-\frac{b_i}{4\pi}\Omega-\frac{b_k\epsilon_{jkm}}{8\pi}\oint_{\mathcal{L}}\left[\delta_{ij}\Delta-\frac{1}{1-\nu}\partial_i\partial_j\right]Z(R)\,dL'_m \tag{B.1}$$

Depending on the particular case, the function $Z(R)$ is

$$Z(R)=\begin{cases} R & \text{classical elasticity}\\ \tilde{R}(R)\approx(1-m)R_{a_1}(R)+mR_{a_2}(R) & \text{Cai's theory (approximately)}\\ A(R) & \text{gradient elasticity of Helmholtz type}\end{cases} \tag{B.2}$$

and Ω is a generalized solid angle

$$\Omega=-\frac{1}{2}\int_S \partial_k\Delta Z(R)\,dA'_k=\int_S v_k\,dA'_k \tag{B.3}$$

In (B.3) we defined the vector:

$$v_k=-\frac{1}{2}\partial_k\Delta Z(R)=\begin{cases} \dfrac{R_k}{R^3} & \text{classical elasticity}\\ \approx(1-m)\dfrac{R_k}{R_{a_1}^3}+m\dfrac{R_k}{R_{a_2}^3} & \text{Cai's theory (approximately)}\\ \dfrac{R_k}{R^3}\left(1-\left(1+\dfrac{R}{\ell}\right)e^{-R/\ell}\right) & \text{gradient elasticity of Helmholtz type}\end{cases} \tag{B.4}$$

We now wish to find the line integral representation of a generalized solid angle. This effort is motivated by the fact that in DD codes, one typically tracks dislocation lines but not slip surfaces and therefore the line integral form of the solid angle is more readily applicable. The derivation presented here generalizes the results of Lazar and Po (2014) because the derivation applies to dislocations having spread core defined by a generic function $Z(R)$. The approach presented here follows the theory of Dirac magnetic monopoles (Wentzel, 1966). The fundamental idea is to transform (B.3) into a line integral via Stokes theorem, which in turn requires that the quantity $v_k=\partial_k\Delta Z(R)$ be written in terms of the curl of a vector potential. However, a complication arises because the divergence of v_k is not vanishing, and therefore a vector potential cannot be found for v_k alone. In fact one can verify that

$$v_{k,k}=-\frac{1}{2}\Delta\Delta Z(R)=\begin{cases} 4\pi\delta(\boldsymbol{x}) & \text{classical elasticity}\\ \approx(1-m)\dfrac{15a_1^4}{R_{a_1}^7}+m\dfrac{15a_2^4}{R_{a_2}^7} & \text{Cai's theory (approximately)}\\ 4\pi G(\boldsymbol{x}) & \text{gradient elasticity of Helmholtz type}\end{cases} \tag{B.5}$$

Nevertheless, introducing a "fictitious" (Wentzel, 1966) vector field v_k^f with the property $v_{k,k}^f=-v_{k,k}$, a vector potential Ψ_k can be found for the divergenceless sum $v_k+v_k^f$. From Helmholtz potential theory, it is known that a unique vector potential satisfying both $\Psi_{k,k}=0$ and $v_k+v_k^f=\epsilon_{klm}\Psi_{m,l}$ exists. Consequently, applying the operator $\epsilon_{ijk}\partial_j$ to both sides of the latter equation shows that the vector potential is the solution of following Poisson equation:

$$-\Delta\Psi_i=\epsilon_{ijk}(v_k+v_k^f)_{,j}=\epsilon_{ijk}v_{k,j}^f \tag{B.6}$$

where, in the last equality, the term $\epsilon_{ijk}v_{k,j}$ was dropped as a consequence of the curl-del identity. On the other hand, the fictitious vector field with the aforementioned desired property can be constructed as[5]

$$v_k^f(\boldsymbol{x}) = \int_{\mathcal{D}} v_{m,m}(\boldsymbol{x}-\boldsymbol{s})\, ds_k = -\frac{1}{2}\int_{\mathcal{D}} \Delta\Delta Z(\boldsymbol{x}-\boldsymbol{s})\, ds_k \tag{B.8}$$

where $\mathcal{D}$ is a curve, known as Dirac string, starting at infinity and ending at the origin. Substituting (B.8) into (B.6), one finds immediately:

$$-\Psi_i = -\frac{1}{2}\epsilon_{ijk}\int_{\mathcal{D}} \partial_j \Delta Z(\boldsymbol{x}-\boldsymbol{s})\, ds_k = \epsilon_{ijk}\int_{\mathcal{D}} v_j(\boldsymbol{x}-\boldsymbol{s})\, ds_k \tag{B.9}$$

Choosing the Dirac string to be a straight line with (constant) unit direction $\hat{\boldsymbol{s}}$ and recalling the definition of v_k given in Eq. (B.4), the vector potential can be found as

$$\begin{aligned}
\Psi_i(\boldsymbol{R}) &= \epsilon_{ijk}\int_{-\infty}^{0} v_k(\boldsymbol{R}-\alpha\hat{\boldsymbol{s}})\hat{s}_j d\alpha = \epsilon_{ijk}\hat{s}_j\int_{-\infty}^{0} v_k(\boldsymbol{R}-\alpha\hat{\boldsymbol{s}})\, d\alpha \\
&= \begin{cases}
\epsilon_{ijk}\hat{s}_j\displaystyle\int_{-\infty}^{0}\frac{R_k-\alpha\hat{s}_k}{|\boldsymbol{R}-\xi\hat{\boldsymbol{s}}|^3}\, d\alpha = \epsilon_{ijk}\hat{s}_j R_k\int_{-\infty}^{0}\frac{d\alpha}{|\boldsymbol{x}-\alpha\hat{\boldsymbol{s}}|^3} & \text{classical elasticity} \\
\approx (1-m)\dfrac{\epsilon_{ijk}\hat{s}_j R_k}{R_{a_1}(R_{a_1}+\hat{s}_p R_p)} + m\dfrac{\epsilon_{ijk}\hat{s}_j R_k}{R_{a_2}(R_{a_2}+\hat{s}_p R_p)} & \text{Cai's theory (approximately)} \\
\epsilon_{ijk}\hat{s}_j x_k\displaystyle\oint_{-\infty}^{0}\frac{1}{|\boldsymbol{x}-\xi\hat{\boldsymbol{s}}|^3}\left(1-\left(1+\frac{|\boldsymbol{x}-\xi\hat{\boldsymbol{s}}|}{\ell}\right)e^{-|\boldsymbol{x}-\xi\hat{\boldsymbol{s}}|/\ell}\right)d\xi & \text{gradient elasticity of Helmholtz type}
\end{cases} \\
&= \begin{cases}
\dfrac{\epsilon_{ijk}\hat{s}_j R_k}{R(R+\hat{s}_p R_p)} & \text{classical elasticity} \\
\approx (1-m)\dfrac{\epsilon_{ijk}\hat{s}_j R_k}{R_{a_1}(R_{a_1}+\hat{s}_p R_p)} + m\dfrac{\epsilon_{ijk}\hat{s}_j R_k}{R_{a_2}(R_{a_2}+\hat{s}_p R_p)} & \text{Cai's theory (approximately)} \\
\epsilon_{ijk}\hat{s}_j x_k\left(\dfrac{1}{x(x+\hat{s}_p x_p)} - \displaystyle\oint_{-\infty}^{0}\frac{1}{|\boldsymbol{x}-\xi\hat{\boldsymbol{s}}|^3}\left(1+\frac{|\boldsymbol{x}-\xi\hat{\boldsymbol{s}}|}{\ell}\right)e^{-|\boldsymbol{x}-\xi\hat{\boldsymbol{s}}|/\ell}\, d\xi\right) & \text{gradient elasticity of Helmholtz type}
\end{cases}
\end{aligned} \tag{B.10}$$

Knowing the vector potential Ψ_i, the generalized solid angle can be transformed using Stokes theorem:

$$\Omega = \oint_{\mathcal{S}} (\epsilon_{ijk}\Psi_{k,j} - v_i^f)\, dA_i = \oint_{\partial\mathcal{S}} \Psi_i dL_i - \Omega^f \tag{B.11}$$

where the "fictitious angle"

$$\Omega^f = \int_{\mathcal{S}} v_i^f\, dA_i = \int_{\mathcal{S}}\int_{\mathcal{D}}\left(-\frac{1}{2}\Delta\Delta Z(\boldsymbol{x}-\boldsymbol{x}')\right)dL_i'\, dA_i \tag{B.12}$$

constitutes the contribution of the fictitious vector field. For the classical case, the fictitious angle is

$$\Omega^f = \int_{\mathcal{S}}\int_{\mathcal{D}} 4\pi\delta(\boldsymbol{x}-\boldsymbol{x}')\, dL_i'\, dA_i = \begin{cases} +4\pi & \text{if the Dirac string crosses the slip surface positively} \\ 0 & \text{if the Dirac string does not cross the slip surface} \\ -4\pi & \text{if the Dirac string crosses the slip surface negatively} \end{cases} \tag{B.13}$$

Therefore it is seen that, for the classical theory, the contribution of the fictitious vector can be ignored if the Dirac string is chosen not to intersect the slip surface. The latter is a convenient property that can be exploited for the numerical calculation of the displacement field of dislocation loops in DD codes based on the classical theory.

However, application of the same property for dislocation loops with spread core soon proves futile. The stumbling stone is the fact that the fictitious angle involves integration of the function $\Delta\Delta Z(\boldsymbol{x}-\boldsymbol{x}')$, which, in general, is non-vanishing for $\boldsymbol{x}\neq\boldsymbol{x}'$. For example, for the gradient solution, the fictitious angle is

$$\Omega^f = \int_{\mathcal{S}}\int_{\mathcal{D}} 4\pi G(\boldsymbol{x}-\boldsymbol{x}')\, dL_i'\, dA_i \tag{B.14}$$

where $G(\boldsymbol{x}-\boldsymbol{x}')$ is the Green's function of the Helmholtz operator. The latter is non-vanishing for $\boldsymbol{x}\neq\boldsymbol{x}'$ and therefore the fictitious angle cannot be ignored even if the Dirac string does not cross the slip surface. Nevertheless, it is true that the fictitious angle vanishes identically if the slip surface is flat and the Dirac string is chosen to lie on a plane parallel to it. This is the condition under which the fictitious angle can be ignored and it should be employed in DD simulations to compute the solid angle as a line integral. Under this condition, the generalized solid angle associated with a dislocation loop with

[5] From the definition (B.8), the property $v_{k,k}^f = -v_{k,k}$ of the fictitious vector can be verified as follows:

$$v_{k,k}^f(\boldsymbol{x}) = \frac{\partial}{\partial x_k}\int_{\mathcal{D}} v_{j,j}(\boldsymbol{x}-\boldsymbol{s})\, ds_k = \int_{\mathcal{D}}\frac{\partial}{\partial x_k}v_{j,j}(\boldsymbol{x}-\boldsymbol{s})\, ds_k = -\int_{\mathcal{D}}\frac{\partial}{\partial s_k}v_{j,j}(\boldsymbol{x}-\boldsymbol{s})\, ds_k = -[v_{j,j}(\boldsymbol{x}-\boldsymbol{s})]_{\infty}^{\boldsymbol{0}} = -v_{j,j}(\boldsymbol{x}) \tag{B.7}$$

spread core is

$$\Omega = \oint_{\partial S} \Psi_i \, dL_i. \tag{B.15}$$

References

Aifantis, E.C., 2009. Non-singular dislocation fields. IOP Conf. Ser.: Mater. Sci. Eng. 3, 012026.
Aubry, S., Kang, K., Ryu, S., Cai, W., 2011. Energy barrier for homogeneous dislocation nucleation: comparing atomistic and continuum models. Scr. Mater. 64 (11), 1043–1046.
Beltz, G.E., Freund, L.B., 1993. On the nucleation of dislocations at a crystal surface. Phys. Status Solidi (b) 180 (2), 303–313.
Brown, L.M., 1964. The self-stress of dislocations and the shape of extended nodes. Philos. Mag. 10 (105), 441–466.
Bulatov, V., Cai, W., Fier, J., Hiratani, M., 2004. Scalable line dynamics in ParaDiS. In: Proceedings of the 2004 ACM/IEEE Conference on Supercomputing.
Cai, W., Arsenlis, A., Weinberger, C., Bulatov, V., 2006. A non-singular continuum theory of dislocations. J. Mech. Phys. Solids 54 (3), 561–587.
Cereceda, D., Stukowski, A., Gilbert, M.R., Queyreau, S., Ventelon, L., Marinica, M.-C., Perlado, J.M., Marian, J., 2013. Assessment of interatomic potentials for atomistic analysis of static and dynamic properties of screw dislocations in W. J. Phys.: Condens. Matter 25, 085702.
Cottrell, A.H., 2002. A brief view of work hardening. In: Nabarro, F.R.N., Duesbery, M. (Eds.), Dislocations in Solids V11. North-Holland, Amsterdam, pp. vii–xvii.
de Wit, R., 1960. The Continuum Theory of Stationary Dislocations. Solid State Phys. 10, 249–292.
de Wit, R., 1981. The displacement field of a dislocation distribution. In: Ashby, M.F., Bullough, R., Hartley, C.S., Hirth, J.P. (Eds.), Dislocation Modelling of Physical Systems. Pergamon Press, Oxford, pp. 304–309.
Dupuy, L., Fivel, M.C., 2002. A study of dislocation junctions in FCC metals by an orientation dependent line tension model. Acta Mater. 50 (19), 4873–4885.
Eringen, A.C., 1977a. Edge dislocation in nonlocal elasticity. Int. J. Eng. Sci. 15 (3), 177–183.
Eringen, A.C., 1977b. Screw dislocation in non-local elasticity. J. Phys. D: Appl. Phys. 10 (5), 671–678.
Eringen, A.C., 1983. On differential equations of nonlocal elasticity and solutions of screw dislocation and surface waves. J. Appl. Phys. 54 (9), 4703–4710.
Eringen, A.C., 1984. On continuous distributions of dislocations in nonlocal elasticity. J. Appl. Phys. 56 (10), 2675–2680.
Eringen, A.C., 2002. Nonlocal Continuum Field Theories, 1st Edition Springer, New York.
Eshelby, J.D., 1982. Aspects of the theory of dislocations. In: Hopkins, H.G., Sewell, M.J. (Eds.), Mechanics of Solids, The Rodney Hill 60th Anniversary Volume. Oxford university press, Oxford, pp. 861–902.
Friedel, J., 1967. Dislocations. Addison-Wesley, Reading, MA.
Gavazza, S.D., Barnett, D.M., 1976. The self-force on a planar dislocation loop in an anisotropic linear-elastic medium. J. Mech. Phys. Solids 24 (4), 171–185.
Ghoniem, N.M., Amodeo, R., 1988. Computer simulation of dislocation pattern formation. Solid State Phenom. 3&4, 377–388.
Ghoniem, N.M., Tong, S., Sun, L., 2000. Parametric dislocation dynamics: a thermodynamics-based approach to investigations of mesoscopic plastic deformation. Phys. Rev. B 61 (2), 913–927.
Gulluoglu, A.N., Srolovitz, D.J., LeSar, R., Lomdahl, P.S., 1989. Dislocation distributions in two dimensions. Scr. Metall. 23 (8), 1347–1352.
Gutkin, M.Y., Aifantis, E., 1996. Screw dislocation in gradient elasticity. Scr. Mater. 35 (11), 1353–1358.
Gutkin, M.Y., Aifantis, E., 1997. Edge dislocation in gradient elasticity. Scr. Mater. 36 (1), 129–135.
Gutkin, M.Y., Aifantis, E.C., 1999. Dislocations in the Theory of Gradient Elasticity. Scr. Mater. 40, 559–566.
Hirth, J.P., Lothe, J., 1992. Theory of Dislocations, 2nd Edition Krieger Publishing Company, Malabar, Florida.
Kessel, S., 1970. Spannungsfelder einer Schraubenversetzung und einer Stufenversetzung im Cosseratschen Kontinuum. Z. Angew. Math. Mech. 50, 547–553.
Kröner, E., 1963. On the physical reality of torque stresses in continuum mechanics. Int. J. Eng. Sci. 1 (2), 261–278.
Kubin, L.P., Canova, G., Condat, M., Devincre, B., Pontikis, V., Bréchet, Y., 1992. Dislocation microstructures and plastic flow: a 3D simulation. Solid State Phenom. 23, 455–472.
Lardner, R.W., 1971. Dislocations in Materials with Couple Stress. IMA J. Appl. Math. 7, 126–137.
Lazar, M., 2012. Non-singular dislocation loops in gradient elasticity. Phys. Lett. A 376 (21), 1757–1758.
Lazar, M., 2014. On gradient field theories: gradient magnetostatics and gradient elasticity. Phil Mag, submitted for publication.
Lazar, M., 2013. The fundamentals of non-singular dislocations in the theory of gradient elasticity: dislocation loops and straight dislocations. Int. J. Solids Struct. 50 (2), 352–362.
Lazar, M., Agiasofitou, E., 2011. Screw dislocation in nonlocal anisotropic elasticity. Int. J. Eng. Sci. 49 (12), 1404–1414.
Lazar, M., Kirchner, H., 2007. The Eshelby stress tensor, angular momentum tensor and dilatation flux in gradient elasticity. Int. J. Solids Struct. 44, 2477–2486.
Lazar, M., Maugin, G.A., 2005. Nonsingular stress and strain fields of dislocations and disclinations in first strain gradient elasticity. Int. J. Eng. Sci. 43 (13–14), 1157–1184.
Lazar, M., Maugin, G.A., 2006. Dislocations in gradient elasticity revisited. Proc. R. Soc. A—Math. Phys. Eng. Sci. 462 (2075), 3465–3480.
Lazar, M., Maugin, G.A., Aifantis, E.C., 2005. On dislocations in a special class of generalized elasticity. Phys. Status Solidi (b) 242 (12), 2365–2390.
Lazar, M., Po, G., 2014. The solid angle and the Burgers formula in the theory of gradient elasticity: line integral representation. Phys. Lett. A 378, 597–601.
Lepinoux, J., Kubin, L.P., 1987. The dynamic organization of dislocation-structures: a simulation. Scr. Metall. Mater. 21 (6), 833–838.
Lothe, J., 1992. Dislocations in continuous elastic media. In: Indenbom, V.L., Lothe, J. (Eds.), Elastic Strain Fields and Dislocation Mobility. North-Holland, Amsterdam, The Netherlands, pp. 175–235.
Madec, R., Devincre, B., Kubin, L.P., 2002. From dislocation junctions to forest hardening. Phys. Rev. Lett. 89 (25), 255508.
Minagawa, S., 1979. Stress and Couple-Stress Fields Produced by Circular Dislocations in an Isotropic Elastic Micropolar Continuum. J. Appl. Math. Mech. (ZAMM) 59 (7), 307–315.
Mindlin, R.D., 1964. Micro-structure in linear elasticity. Arch. Ration. Mech. Anal. 16 (1), 51–78.
Mindlin, R.D., 1972. Elasticity, piezoelectricity and crystal lattice dynamics. J. Elast. 2 (4), 217–282.
Mindlin, R.D., Eshel, N.N., 1968. On first strain-gradient theories in linear elasticity. Int. J. Solids Struct. 4, 109–124.
Mura, T., 1987. Micromechanics of Defects in Solids, 2nd Edition Kluwer Academic Publishers, Dordrecht, The Netherlands.
Nabarro, F.R.N., 1947. Dislocations in a simple cubic lattice. Proc. Phys. Soc. 59 (2), 256–272.
Nabarro, F.R.N., 1987. Theory of Crystal Dislocations. Dover Publications, New York.
Nowacki, W., 1986. Theory of Asymmetric Elasticity. PWN-Polish Scientific Publishers, Warszawa.
Peach, M., Koehler, J., 1950. The forces exerted on dislocations and the stress fields produced by them. Phys. Rev. 80 (3), 436–439.
Peierls, R., 1940. The size of a dislocation. Proc. Phys. Soc. 52 (1), 34–37.
Plimpton, S., 1995. Fast parallel algorithms for short-range molecular-dynamics. J. Comput. Phys. 117 (1), 1–19.
Po, G., et al., 2013. Mechanics of defect evolution library (model). ⟨https://bitbucket.org/model/model/wiki/Home⟩.
Po, G., Ghoniem, N., 2014. A variational formulation of constrained dislocation dynamics coupled with heat and vacancy diffusion. J. Mech. Phys. Solids 66, 103–116.
Schoeck, G., 2010. Atomic dislocation core parameters. Phys. Status Solidi B 247 (2), 265–268.

Schwarz, K.W., 1997. Interaction of dislocations on crossed glide planes in a strained epitaxial layer. Phys. Rev. Lett. 78 (25), 4785–4788.
Shenoy, V.B., Kukta, R.V., Phillips, R., 2000. Mesoscopic analysis of structure and strength of dislocation junctions in fcc metals. Phys. Rev. Lett. 84 (7), 1491–1494.
Shin, C.S., Fivel, M.C., Rodney, D., Phillips, R., Shenoy, V.B., Dupuy, L., 2001. Formation and strength of dislocation junctions in FCC metals: a study by dislocation dynamics and atomistic simulations. J. Phys. IV Fr. 11 (PR5), 19–26.
Teodosiu, C., 1982. Elastic Models of Crystal Defects. Springer Verlag, Berlin.
Toupin, R.A., Gazis, D.C., 1965. Surface effects and initial stress in continuum and lattice models of elastic crystals. In: Wallis, R.F. (Ed.), Proceedings of the International Conference on Lattice Dynamics held at Copenhagen, Denmark, August 5–9, 1963, pp. 597–605.
Volterra, V., 1907. Sur l'equilibre des corps elastiques multiplement connexes. Ann. Sci. l'Ecole Norm. Suprieure 24, 401–517.
Wentzel, G., 1966. Comments on Dirac's theory of magnetic monopoles. Progr. Theor. Phys. Suppl. 37 (Supplement 1), 163–174.
Weygand, D., 2002. Aspects of boundary-value problem solutions with three-dimensional dislocation dynamics. Model. Simul. Mater. Sci. 10 (4), 437–468.
Wickham, L., Schwarz, K.W., Stölken, J., 1999. Rules for forest interactions between dislocations. Phys. Rev. Lett. 83, 4574–4577.
Zbib, H., Rhee, M., Hirth, J., 1998. On plastic deformation and the dynamics of 3D dislocations. Int. J. Mech. Sci. 40, 113–127.